

Alma Mater Studiorum Università di Bologna
Archivio istituzionale della ricerca

Deposition processes over complex topographies: Experimental data meets atmospheric modeling

This is the final peer-reviewed author's accepted manuscript (postprint) of the following publication:

Published Version:

Laura, T., Beatrice, M., Enrico, D., Pietro, M., Erika, B., Bartolomeo, S., et al. (2020). Deposition processes over complex topographies: Experimental data meets atmospheric modeling. SCIENCE OF THE TOTAL ENVIRONMENT, 744, 1-12 [10.1016/j.scitotenv.2020.140974].

Availability:

This version is available at: <https://hdl.handle.net/11585/767144> since: 2020-07-27

Published:

DOI: <http://doi.org/10.1016/j.scitotenv.2020.140974>

Terms of use:

Some rights reserved. The terms and conditions for the reuse of this version of the manuscript are specified in the publishing policy. For all terms of use and more information see the publisher's website.

This item was downloaded from IRIS Università di Bologna (<https://cris.unibo.it/>).
When citing, please refer to the published version.

(Article begins on next page)

This is the final peer-reviewed accepted manuscript of:

Laura Tositti, Beatrice Moroni, Enrico Dinelli, Pietro Morozzi, Erika Brattich, Bartolomeo Sebastiani, Chiara Petroselli, Stefano Crocchianti, Roberta Selvaggi, Goretti Enzo, David Cappelletti (2020). Deposition processes over complex topographies: Experimental data meets atmospheric modeling, Science of The Total Environment, Volume 744

The final published version is available online at
<https://dx.doi.org/10.1016/j.scitotenv.2020.140974>

Rights / License:

The terms and conditions for the reuse of this version of the manuscript are specified in the publishing policy. For all terms of use and more information see the publisher's website.

This item was downloaded from IRIS Università di Bologna (<https://cris.unibo.it/>)

When citing, please refer to the published version.

Deposition processes over complex topographies: experimental data meets atmospheric modeling

Tositti Laura^{1*}, Moroni Beatrice², Dinelli Enrico^{3,4}, Morozzi Pietro¹, Brattich Erika⁵, Sebastiani Bartolomeo², Petroselli Chiara⁶, Crocchianti Stefano², Selvaggi Roberta², Goretti Enzo², Cappelletti David²

¹ Department of Chemistry “G. Ciamician”, University of Bologna, Bologna (BO), 40126, ITALY

² Department of Chemistry, Biology and Biotechnologies, University of Perugia, Perugia (PG), 06123, ITALY

³ Department of Biological, Geological and Environmental Sciences (BiGeA), University of Bologna, Bologna (BO), 40126, ITALY

⁴ Department of Biological, Geological and Environmental Sciences (BiGeA), U.O.S. Ravenna, Ravenna (RA), 48123, ITALY

⁵ Department of Physics and Astronomy, University of Bologna, Bologna (BO), 40126, Bologna (BO), ITALY

⁶ Faculty of Engineering and Physical Sciences, University of Southampton, 12 University Road, SO17 1BJ Southampton, UK

***Corresponding author:** Laura Tositti

e-mail address: laura.tositti@unibo.it

mailing address: Via Selmi 2, 40126 Bologna (ITALY)

Telephone: +39 051 2099488

Abstract

The present paper describes the assessment of the atmospheric deposition processes in a basin valley through a multidisciplinary approach based on the data collected within an extensive chemical-physical characterization of the soils, combined with the local meteorology. Surface soil cores were collected on a NNW-SSE transect across the Terni basin (Central Italy), between the Monti Martani and the Monti Sabini chains (956 m a.s.l.), featuring the heavily polluted urban and industrial enclave of Terni on its bottom. Airborne radiotracers, namely ^{210}Pb and ^{137}Cs , have been used to highlight atmospheric deposition.

We observed an increased deposition flux of ^{210}Pb and ^{137}Cs at sites located at the highest altitudes, and the associated concentration profiles in soil allowed to evaluate the role of atmospheric deposition.

We also obtained a comprehensive dataset of stable anthropogenic pollutants of atmospheric origin that showed heterogeneity along the transect. The behavior has been explained by the local characteristic of the soil, by seeder-feeder processes promoted by the atmospheric circulation, and was reconciled with the concentration profile of radiotracers by factor analysis. Finally, the substantial impact of the local industrial activities on soil profiles and the role of the planetary boundary layer has been discussed and supported by simulations employing a Lagrangian dispersion model.

1 Introduction

Soil plays a fundamental role in environmental biogeochemical cycling through a wide range of different processes, both naturally and anthropogenically driven. It is characterized by endogenous processes such as soil development, use, and management, as well as by exogenous processes e.g., climatic factors, atmospheric deposition, and runoff, which may add complexity in terms of chemical components transfer, mixing and reworking on not easily predictable space and time scales. As a result, soil behaves as a receptor for atmospheric deposition, reflecting the influence of atmospheric aerosols with the mediation of wet and, to a lesser extent, dry scavenging according to local climatology and pluviometric regime. Atmospheric deposition flux includes numerous chemical species from gas-to-particle reactions derived nutrients such as nitrate, ammonium, and sulfate, to metals, metalloids, and carbonaceous species (Vet et al., 2014a, b). Once deposited, substances may permeate and migrate to depth throughout the soil pores as a function of the relative interaction strength with soil components. Therefore, each atmospherically originated chemical species will produce a vertical concentration profile reflecting the interplay among its own physicochemical properties and soil properties. In particular, the mobility and adsorption processes of a pollutant in soil will depend on the soil mineralogical composition, porosity, water, and organic matter content, pH, and redox conditions. As time goes by, soil itself will evolve leading to temporal accretion and burial of older layers wherein both endogenous and exogenous substances can be stored and redistributed (Vet et al., 2014a; Fowler et al., 2004; Kaste et al., 2003; Lamborg et al., 2000).

Owing to both the morphology and intrinsic complexity of the soil chemical matrix, the assessment of atmospherically-derived components in a soil profile is usually a challenging task because they represent a minor fraction as compared to bulk soil components. In this context, however, environmental radionuclides represent an exception, since both natural and artificial radioisotopes have been historically investigated to trace the fate of atmospheric pollution in depositional

74 environments including soil matrices, posing the basis for modern biogeochemistry, geophysical
75 radiotracer research, and geochronology (Baskaran, 2011).

76 The efficacy of natural and artificial radiotracers in environmental investigations is based on two
77 substantial properties. Firstly, radiotracers can be measured very accurately, even at their lowest
78 molar concentration on a routine basis. Secondly, they are emitted by unambiguous sources, which
79 make them easily recognizable and widely used as surrogates of stable pollutants or as
80 geochronometers and radiotracers (Landis et al., 2016; Fowler et al., 1995; Graustein and Turekian,
81 1986).

82 Soil contains two main groups of radionuclides: geogenic radionuclides, intrinsically associated to
83 the soil parent material, and atmospherically derived radionuclides, transferred to the soil
84 environment through wet and dry deposition. Geogenic radionuclides are mainly represented by
85 uranium and thorium families together with the primordial ^{40}K . The atmospherically derived fraction
86 includes among others ^{210}Pb ($t_{1/2} = 22.3$ years) and ^{137}Cs ($t_{1/2} = 30.2$ years) both widely employed in
87 the study of depositional processes (Baskaran, 2011); ^7Be ($t_{1/2} = 55$ d) is another frequently used
88 atmospheric radiotracer, but owing to the relatively short half-life its use is conditioned by the time
89 elapsed between sampling and measurement.

90 While ^{137}Cs is an artificial radionuclide deriving from both the global fallout (peak emissions from
91 nuclear weapon testing in 1963) and, in the northern hemisphere, from the Chernobyl accident in
92 1986 (IAEA, 2006), ^{210}Pb is a natural radionuclide from the ^{238}U radioactive family including ^{222}Rn
93 and ^{210}Pb formed at intermediate stages of the radioactive chain. In particular, ^{210}Pb belongs to ^{222}Rn
94 progeny, but differently from the parent nuclide which is a noble gas, all its progeny including ^{210}Pb ,
95 is particle reactive and similarly to ^{137}Cs , gets efficiently associated to submicron aerosol particles,
96 tracing airborne particulate and eventually the aerosol sinks (Graustein and Turekian 1989; Preiss
97 et al., 1996; Persson and Holm, 2011; Mabit et al., 2014; Landis et al., 2014). All these radionuclides

98 are highly particle-reactive. Therefore, after being produced/emitted to the air, they quickly get
99 associated with ambient aerosol, usually in the accumulation mode (i.e., submicrometric in size),
100 with a residence time of the order of days up to a few weeks. As a result, they are excellent tracers
101 of both atmospheric aerosol (Tositti et al., 2014a; Brattich et al., 2015a, b; 2016), and of atmospheric
102 deposition (Battiston et al., 1987; Bettoli et al., 1995; Tositti et al., 2006).

103 Airborne radionuclides establish negative concentration gradients in soil with depth. These profiles
104 reflect both their origin and the processes they undergo within the soil, linked to its properties and
105 management. Atmospherically deposited radionuclides are in most cases confined in the upper 15-
106 20 cm of soil which outlines the need for high-resolution sectioning when dealing with soil and the
107 possibility of efficiently detect the influence of atmospheric contribution independently on the
108 nature of the pollutant investigated, as reported in the literature (Suchara et al., 2016, Landis et al.,
109 2014; Graustein and Turekian, 1989).

110 Radionuclides profiles in soil depend on the extent of atmospheric deposition, which in turn
111 depends on a number of meteorological processes and orographical features. In fact, many studies
112 have observed how the deposition rate of wet-removed chemical species increases with increasing
113 altitude. In areas characterized by complex topographies, this differential behavior has been
114 attributed to the influence of orographic clouds which produce an enrichment in aerosol particles
115 being removed by nucleation through the so-called “seeder-feeder mechanism” (see for example
116 Le Roux et al., 2008 and Likuku, 2006 and references therein). Airborne radiotracers, whose
117 environmental sources and sinks are known in remarkable detail, have been successfully applied to
118 constrain the fate of stable substances and pollutants with similar environmental behavior
119 contributing to enlighten their atmospheric source (Vet et al., 2014a; Fowler et al., 2004; Kaste et
120 al., 2003; Lamborg et al., 2000).

121 The present paper concerns the assessment of the depositional pollution features in the Terni basin,
122 an area heavily impacted by human activities in Umbria, Central Italy. The present investigation of
123 biogeochemical cycling of pollutants in the Terni area, accounting for its topographical complexity,
124 is part of a comprehensive environmental study where earlier research shed light on the role of the
125 planetary boundary layer in atmospheric dispersion of pollution in the area (Moroni et al., 2012,
126 2013; Ferrero et al., 2012, 2014). The present work describes the assessment of the atmospheric
127 deposition processes in the Terni basin through a multidisciplinary approach based on the data
128 collected within an extensive chemical-physical characterization of Terni soils, combined with the
129 local meteorology. Specifically, this paper is based on a transect of surface soil cores collected at ten
130 stations along with a mountainous profile across the Terni basin. At each station, radionuclide,
131 inorganic, and organic components concentrations were determined as a function of station height
132 and soil depth. Finally, their connections with atmospheric deposition have been analyzed.

133 The paper is organized as follows:

- 134 • assessment of radionuclidic and chemical vertical profiles at the ten sampling stations;
- 135 • identification of atmospheric inputs of radionuclides and station classification by
136 multivariate techniques;
- 137 • assessment of differential depositional behavior with elevation;
- 138 • qualitative comparison between experimental results and the numerical outputs of a
139 Lagrangian Gaussian puff dispersion model.

140

141

142

143

144

2. Materials and methods

2.a. Site description and sample collection

The Terni district is a densely populated and industrialized area located at the margins of the Central Apennines range in Umbria, Central Italy (Figure 1). The town of Terni (170 m a.s.l.) lies in a vast plain area (about 2% of the territory) surrounded by medium-range geographical elevations (average elevation 800-1200 m).

The local climate is classified as Csa (Köppen classification), i.e., as mid-latitude temperate, with warm, humid summers and cold rainy winters. The mean annual temperature is 14.5 °C, while yearly mean rainfall is 854 mm/y (ARPA-Umbria, 2013). Weak winds, due to the local topography, are typically oriented along the course of the Nera river, predominantly along with the N-NE, NE, and S-SW directions (Meloni and Carpine, 2004). Terni began its industrial development as far back as 1884, with the building of the Italian largest forge, for the production of armor and guns for the Navy. Since then the Acciai Speciali Terni (AST) became the strongest industrial asset of the area, focusing on stainless steel production for more than one hundred years, until the most recent owner, Tyssen-Krupp. Besides the steel industry, three waste incinerators are located in the Terni area for industrial and municipal waste management. Previous assessments on the local source profile identified traffic and agricultural activities as significant contributions of both fine and coarse particulate (Moroni et al., 2012). Considerable efforts have been made to mitigate the impact of industrial emissions, wood-burning, and road traffic, but only a modest improvement of air quality standards has been achieved so far. In particular, long-lasting high pollution level events are frequently observed in the cold season, in association with intense thermal inversion episodes (Ferrero et al., 2012, 2014; Moroni et al., 2013).

167 Soil was sampled in summer 2014 at 10 stations located along a roughly NNW-SSE transect
168 crossing the whole Terni basin roughly along a parabolic section with the bottom coinciding with
169 the Terni urban area in the valley (Figure 1 and Table 1).

170 The stations are classified into three main groups:

- 171 • Stations located close to the main pollution sources within the urban territory (Prisciano-
172 PRI, Pineta Centurini-PCE, and Le Grazie-LGR);
- 173 • Stations located north and south from the main emission area, but at a higher elevation
174 and distance from the direct influence of the pollution sources (Torre Maggiore-MTM, S.
175 Erasmo-ERA, Cesi-CES to the north, Miranda-MIR, Larviano-LAR and Piani di Stroncone-STR
176 south from Terni);
- 177 • Mt. Martano-MM (1094 m a.s.l.), at about 45 km north of Terni is a background mid-
178 altitude station chosen as reference site distant from pollution sources and influenced by
179 the boundary layer only during summertime (Moroni et al., 2015).

180 M. Torre Maggiore (IT5220013) and Piani di Stroncone (IT5220021) are Natura 2000 protected
181 areas (<https://natura2000.eea.europa.eu/>, accessed 21/04/2020).

182 At each station, 3 shallow cores 20 cm long were drilled using a PTFE liner (diameter = 7 cm) and
183 sectioned every 5 cm. Soil samples were air-dried in a low humidity environment for about 2
184 weeks in a hood, then crushed and sieved (2 mm certified mesh).

185 Each core was splitted and one portion of the sample was weighed and oven-dried at 105 °C for 16
186 hours and then weighted again to determine the residual moisture.

187 According to the documentation on soil management available through the local administration, all
188 the Terni area is characterized by a high degree of human exploitation. The basic information about

189 the sampling stations as well as information about the bedrock lithology, recovered and classified
190 using the layer “geology of Italy” downloaded from the “Portale Cartografico Nazionale”
191 (<http://www.pcn.minambiente.it/mattm/servizio-di-scaricamento-wfs/>, accessed 21/04/2020), is
192 reported in Table 1.

193

194 2.b. Analytical methods

195 2.b.1. Elemental analysis by WD-XRF analysis

196 Soil samples were further homogenized and milled in an agate mortar to obtain the fraction < 10
197 μm . Powder pellets were prepared for the XRF analysis to determine major and trace element
198 concentrations with a Panalytical Axios4000 spectrometer equipped with a Rh tube. Matrix
199 corrections were applied during data processing (Franzini et al., 1972, 1975). Precision and accuracy
200 for trace element determination were better than 5% except for elements at 10 ppm or lower (10-
201 15%), as estimated from the analysis of international reference materials (Lancianese and Dinelli,
202 2016). The investigated chemical components include SiO_2 , TiO_2 , Al_2O_3 , Fe_2O_3 , MnO , MgO , CaO ,
203 Na_2O , K_2O , P_2O_5 , As, Ba, Ce, Co, Cr, Cu, Ga, La, Mo, Nb, Ni, Pb, Rb, S, Sc, Sn, Sr, Th, V, Y, Zn, Zr. The
204 minimum and maximum values at each sampling station are reported in Table S1 of the
205 Supplementary Material (hereafter SM).

206

207 2.b.2. High-resolution γ -ray spectrometry

208 Natural and artificial radionuclides including among others ^{210}Pb ($E_\gamma = 46.5 \text{ keV}$), ^{226}Ra ($E_\gamma = 186 \text{ keV}$)
209 and ^{137}Cs ($E_\gamma = 661.7 \text{ keV}$) were determined in soil samples by a HPGe (High Purity Germanium)
210 extended-range detector (PROFILE Hyper Pure Germanium detector by Ortec-Ametek Inc.). The
211 detector (relative efficiency of 20% and resolution (Full Width at Half Maximum, FWHM) of 1.9 keV
212 at 1332.5 keV) was calibrated for energy and efficiency using a multiple radionuclide liquid source

(DKD, Eckert & Ziegler Nuclitec GmbH) in a jar geometry (diameter = 54 mm and thickness = 1 cm). Soil samples were measured in the same jar geometry, weighed and then counted for 24 hours each to optimize peak counting statistics. Spectra were subsequently analysed with Gamma Vision-32 software (version 6.07, Ortec-Ametek) allowing also for self-attenuation at low energy on the basis of the apparent density. ^{226}Ra activity was determined at 186 keV correcting the peak area for ^{235}U emission according to the procedure reported by Gilmore (2008). Atmospheric ^{210}Pb defined as $^{210}\text{Pb}_{\text{ex}}$, i.e. “in excess” of the fraction supported by in situ production by ^{226}Ra , was calculated by subtracting the activity fraction of ^{210}Pb in equilibrium with ^{226}Ra from the mineral soil component from the total ^{210}Pb detected in each sample (Swarzenski, 2014), after correcting for self-absorption. Further details on γ -spectrometry determinations are available elsewhere (Cinelli et al., 2014; Tositti et al., 2016). Uncertainty (here defined as one standard deviation) on the γ photopeaks was calculated propagating the error resulting from the efficiency calibration fit previously determined over the counting error. Minimum detectable activity (MDA) was determined using the Traditional ORTEC method (ORTEC, 2003) with a peak-cut-off limit of 40%. Analytical quality control has been assessed using certified reference materials DH-1a and UTS-3, both by CANMET. The minimum and maximum radionuclides concentration data are reported in Table S2 of the SM.

229

230 *2.b.3. PAHs and n-alkanes*

The determination of PAHs and n-alkanes were performed by GC-MS on a Varian-Chrompack 3800 gas-chromatograph coupled with a tandem mass spectrometry ion trap detector (ITD-MS) (Varian Saturn 2000) and equipped with a split–splitless inlet and a low bleed Factor Four VF-5ms analytical capillary column (Chrompack). The analytical procedure was described in detail in Cartechini et al. (2015). PAHs and n-alkanes concentration data analysed in Terni soils are reported in Table S3 of the SM.

237 *2.b.4. Loss-On-Ignition LOI, TOC and N*

238 Total loss on ignition (LOI) was gravimetrically estimated after overnight heating on 1 gram of
239 sample at 950 °C in a muffle furnace.

240 A LECO Truspec CN analyzer was employed for the determination of total organic carbon (TOC) and
241 total nitrogen (N). About 20 mg of soil sieved at 0.5 mm were weighed in a tin capsule. TOC was
242 obtained by difference to between total carbon and inorganic carbon made on the same samples
243 kept in the muffle for 5 hours at 550 ° C. The accuracy at which the instrument operates is 0.3 ppm
244 or 0.5% RSD for carbon and 40 ppm 0.5% RSD for nitrogen. LOI, TOC, and N data are reported in
245 Table S1 of the SM.

246

247 *2.c. Statistical methods and elaboration tools*

248 *2.c.1. Principal Component Analysis (PCA) and Gabriel Biplot*

249 Factor Analysis based on Principal Component Analysis (PCA) was applied to the complete transect
250 dataset derived from the application of the analytical techniques detailed above, with the aim of
251 classifying soil samples and assessing similarities/differences among the sampling stations.

252 Missing data or data below detection limits (LOD) were substituted in the data matrices by LOD/2
253 in order to optimize the modelling outcome. The dataset was normalized before performing PCA by
254 means of autoscaling, i.e. subtracting the mean value to each observation and dividing by the
255 standard deviation. This process produces new variables with zero mean and unit standard
256 deviation, so that each of them has the same importance regardless their original variances and
257 units of measure as explained by van den Berg et al. (2006) and Jolliffe et al. (2016).

258 Gabriel biplot (Gabriel, 1971) was also used in order to represent both variables and cases together
259 in two dimensions.

260 2.c.2. CALPUFF

261 Calpuff is a Lagrangian Gaussian Puff model and has been one of the preferred models adopted for
262 regulatory purposes to assess pollutants transport in the range from tens to hundreds of kilometers
263 (USEPA, 2005). Similar to other Lagrangian models, it is still recommended as a screening model
264 (USEPA, 2017). Its advantage over gaussian-based models is based on its capability to simulate the
265 transport of pollutants in calm and stagnant condition (Daly, 2007), i.e. eventually those typically
266 affecting the Terni valley.

267 The Calpuff dispersion model (version 7.2.1) was used in the present work in combination with
268 CALMET (version 6.327), a diagnostic meteorological model that develops wind and temperature
269 fields on a three-dimensional gridded domain. Associated two-dimensional fields such as mixing
270 height, surface characteristics, and dispersion properties are also included in its output file.

271 The domain of the simulation was a square grid 20 km wide centered on the Terni city. The
272 meteorological data was produced by ARPA Emilia Romagna for the year 2014 on the basis of the
273 LAMA (Limited Area Meteorological Analysis) dataset (Jungen et al., 2006) that covers the Italian
274 territory and the surrounding regions with a horizontal resolution of 0.0625° (~ 7 km) and a temporal
275 resolution of 1 hour. Boundary conditions were provided by the global scale analysis model ECMWF.
276 The diagnostic model requires both geophysical and meteorological data. Among the former ones,
277 terrain elevations were derived from Umbria high-resolution regional thematic cartography, the 25
278 m resolution Digital Terrain Models of regional coverage. Domain points falling outside Umbria were
279 obtained from the 3 arc-seconds Shuttle Radar Topography Mission dataset. The land-use categories
280 were computed starting from the Corine Land Cover 2000 (22 Oct 2009 update).

281 Calpuff model allows to specify the source size and type, as well as to assume the source emission
282 as constant or variable in a known mode according to cycle, time of the day, year, etc. (see the
283 discussion, in the following).

284 The code resolution enables to account for spatial inhomogeneities deriving from orography
285 localized land use as well as wind circulation and pollutants dispersion in the domain, leading to
286 adequately reproduce calm and breeze regimes. Moreover, the use of a Lagrangian dispersion
287 model allows to evaluate the effects both in proximity and at distance from the simulated sources,
288 including the area of maximum fallout of total suspended particles (TSP). Results of the Calpuff
289 model are expressed as soil concentrations isopleths. In this work, we chose to evaluate mean
290 annual concentrations and maximum daily concentrations. This last value produces the maximum
291 annual value reached by the pollutant in each cell (side 200x200 m).

292 Most of the Calpuff technical options were left to the default settings. However, for the purposes
293 of this work, we chose to simulate the vertical wind shear, without considering the chemical
294 transformation from source to receptor, and to calculate the dispersion coefficients from the values
295 of micrometeorological variables. As far as the PM10 size parameters for dry deposition are
296 concerned, a geometric mass mean diameter of 0.48 micrometers with a geometric standard
297 deviation of 2.0 micrometers was selected.

298 In the CALPUFF simulation, we included as a source only the major industrial plant of the region, the
299 AST steel plant. The plant stacks were modeled as constant 47 points sources. The emission rates
300 adopted were proposed by the plant operator in the Application for Site Certification submitted in
301 2010 or the certified self-monitored concentrations of the emission gases for the year 2010. This
302 source configuration is deemed emitting 96% of NOx and PM10 mass on an annual basis. Since each
303 source was assumed to emit at the highest constant rate for the whole period, the simulation could
304 be considered as a worst-case scenario. However, fugitive emissions such as those associated with
305 the volatilization and vapor emission from open vessels and the releases from materials handling,
306 especially the north-east on-site disposal, were not included.

307

308 **3. Results and discussion**

309 *3.a. Atmospheric radionuclides and depositional patterns*

310 In this work, the radionuclides ^{137}Cs and $^{210}\text{Pb}_{\text{ex}}$ have been determined in a series of ten surface
311 soil profiles to trace the occurrence and the extent of stable pollution fallout across the study
312 area. These radiotracers have been detected at all the stations investigated, suggesting that the
313 influence of atmospheric deposition is active across the whole Terni district.

314 In order to outline different depositional patterns among the stations, concentration vertical
315 profiles and inventories of both radiotracers were examined. ^{137}Cs and $^{210}\text{Pb}_{\text{ex}}$ activity
316 concentration depth profiles are reported in Figure 2.

317 At best, an undisturbed profile of atmospheric ^{210}Pb shows a monotonic decrease with depth, a
318 situation controlled mainly by the organic fraction to which this radionuclide (as well as the
319 corresponding element) is firmly bound, leading even the possibility of dating when high-resolution
320 sectioning is carried out (Landis et al., 2016). Differently from ^{210}Pb , ^{137}Cs shows ideally two distinct
321 activity peaks corresponding to the 1963 and 1986 horizons, well preserved in the case of
322 undisturbed depositional environments; this is not granted in soil wherein the complex behavior of
323 this radionuclide is hardly predictable, especially when long time from deposition has elapsed. ^{137}Cs
324 can be initially bound to surface organics from vegetable litter and subsequently released through
325 rain permeation leading to a lagged association to the clay and organic components fractions at
326 depth as described in detail in Suchara et al. (2016). However, vertical profiles of radionuclides along
327 a soil profile at every single location reflect their behavior in terms of physicochemical interaction
328 between the mobile phase(s) containing the radionuclides and the solid matrix; also the
329 perturbation (disturbance) caused by local soil management, if any, can play a role.

330 In most cases, soil concentration for both airborne radionuclides showed maxima in the top layer
331 confirming the influence of active deposition from the atmospheric compartment. In most of the
332 profiles, concentrations monotonically decreased as a function of the depth. In some cases, the
333 decrease was noteworthy for ^{137}Cs , even down to the fourth layer. ^{137}Cs , a monovalent soft cation,
334 has a greater vertical mobility and showed consistently a broader distribution with respect to
335 $^{210}\text{Pb}_{\text{ex}}$. Thanks to its strong association with the soil organic fraction, $^{210}\text{Pb}_{\text{ex}}$ is on average less
336 mobile than ^{137}Cs , remaining usually confined in the uppermost first and second layers (Mabit et al.,
337 2014; Suchara et al., 2016).

338 Altogether, the profiles of the two radiotracers also reflect different post-depositional behavior
339 contributing to a more complete understanding of the atmosphere/soil relationships. The most
340 disturbed (i.e. not decreasing) radiotracer profiles are those collected at the bottom stations (i.e.
341 PRI, LGR, and PCE) all in proximity of residential and/or industrial sides. Specifically, the high degree
342 of perturbation at LGR and PRI largely results from the strong anthropogenic influence from urban
343 and industrial activities. In particular, PRI is in the core of the industrial Terni district while LGR is
344 located in the Terni residential area, connecting the randomized distribution of radionuclides to the
345 local remarkable degree of soil disturbance from human activities (e.g., reworking). On the other
346 side, PCE maintains a slight degree of atmospheric deposition identifiable by the decreasing
347 concentration trend with depth. Atmospheric deposition at PCE is sensibly affected by the airshed
348 of Terni conurbation in terms of chemical composition and is possibly supported by the pine stand,
349 a park area dating back about fifty years ago. Atmospheric deposition is therefore detectable in the
350 area owing both to the absence of soil reworking in the last five decades whereas throughfall and
351 foliar interception may have played a role in soil enrichment of the fallout species (Fowler et al.,
352 2004; Likuku et al., 2006).

353 These differences in concentration vs. depth profiles arise mainly from the distinct soil
354 characteristics. For this reason, depth profiles of atmospheric radionuclides have been evaluated
355 individually for each sampling station. In order to assess the extent of deposition rate, comparing
356 the different stations, we calculated the radionuclide inventory, a parameter conceptually close to
357 a depositional flux. The inventory, expressed in Bq/m^2 , is the integral of the radionuclide activity
358 concentration over depth accounting for soil geometry (unit surface and layer thickness) and soil
359 mass density, and was calculated according to the method proposed by Graustein and Turekian
360 (1986, 1989).

361 The results are reported in Figure 3 where ^{137}Cs and $^{210}\text{Pb}_{\text{ex}}$ inventories are represented along a
362 profile cross section. Minimum inventories are observed at the three valley bottom stations while
363 maxima are observed at the three most elevated stations, namely at MTM, and, with slightly lower
364 values, at MM to the north and STR on the opposite branch of the transect (see Figure 1). These
365 results are in agreement with previous studies observing an increased deposition flux with height
366 (Fowler et al., 1988; Le Roux et al., 2008; Stankwitz et al., 2012; Blackwell and Driscoll, 2015).

367 Atmospheric deposition appears to be higher on the NNW side of the transect with respect to the
368 SSE side, with the exception of ERA station where both ^{137}Cs and $^{210}\text{Pb}_{\text{ex}}$ inventories are lower
369 possibly due to local disturbances.

370 This difference in the inventories has been evaluated by the Unpaired Two-Samples Wilcoxon Test
371 at a significance level of 95%. This non-parametric test allows to compare the means in two
372 independent groups of samples without any prior assumption regarding data distribution. The
373 results of the test indicate a statistically significant difference between the NNW (defined by MM,
374 MTM, and ERA stations) and the SSE (defined by PRI, PCE, and LGR stations) sides of the Terni
375 transect (p-value less than 0.05 for both ^{137}Cs and $^{210}\text{Pb}_{\text{ex}}$) and the exceedance in deposition in the

376 NNW side might be due to the combination of the meteorological conditions of the district, of the
377 dominant circulation pattern along the transect under the influence of both mesoscale and
378 mountain/valley breeze regime (see further on in this paper), as well as of the distinct origin of the
379 two radionuclides. In fact, while ^{137}Cs has been emitted in a pulsed way by point sources and its
380 transport through the troposphere over the investigated region has occurred well above the
381 atmospheric boundary layer, $^{210}\text{Pb}_{\text{ex}}$ is generated in the lowest layers of the troposphere through
382 radon exhalation and decay, which means a continuous and extended source area. As a result, it
383 cannot be excluded that $^{210}\text{Pb}_{\text{ex}}$ deposition flux is contributed by both local and distant sources. As
384 such, the former component may be affected by the seeder-feeder phenomenology through the
385 uplift of radon enriched air masses from the plain, while the latter can be supported also by
386 mesoscale/synoptic processes.

387 As a whole, we can conclude that the radionuclidic signature traces the atmospheric deposition
388 along the soil transect in a fairly satisfactory way, though with differences that deserve a thorough
389 inspection and evaluation.

390

391 *3b. Sampling stations and their association with atmospheric radiotracers*

392 We will focus herein on the strategy adopted for detecting associations between atmospheric
393 radiotracers and sampling stations. Owing to the extensive dataset collected, a multivariate
394 approach was selected in order to detect data patterns and significant associations as widely applied
395 in atmospheric science (e.g., Tositti et al., 2014b, 2018a; Núñez-Alonso et al., 2019, Petroselli et al.,
396 2019) and in general in environmental science (e.g., Perez-Bendito and Rubio, 1999).

397 Factor analysis based on Principal Component Analysis (PCA) was applied to compositional data
398 including the atmospherically derived radionuclides from all stations and in all the sections for

station classification and solved for station affinity; Gabriel biplot showing the two atmospheric radionuclides ($^{210}\text{Pb}_{\text{ex}}$ and ^{137}Cs) is reported in Figure 4, while factor scores (that are the observations coordinates on the PCA dimensions) are reported in Table 2. While each soil station has its own peculiarities, and will be object of a dedicated paper, the station score distribution shows that all the stations are clustered in groups reflecting substantially their mean height. Similarities are found between MM and MTM, i.e. the high-altitude stations on the NNW branch of the transect, and between STR and MIR on the opposite edge, in connection with minimal human disturbances as compared to bottom stations. A second larger group includes CES, LGR, LAR, PRI, i.e. the stations at low-altitude within the transect, while PCE and ERA appear as isolated with respect to all the others. Figure 4 shows as PC1 is poorly described by atmospheric radiotracers ($^{210}\text{Pb}_{\text{ex}}$ and ^{137}Cs), unlike PC2 and PC3. The use of $^{210}\text{Pb}_{\text{ex}}$ and ^{137}Cs suggests a clear separation among the ERA, MIR, and PRI stations, which conversely does not appear among the PCE, MM, and MTM.

The distinction of the ERA station is in agreement with what previously observed. Also, the PRI station can be justified by an anomaly in the concentration profiles of both ^{210}Pb and ^{137}Cs , which is correlated with disturbances related to local soil use (see Figure 2 and Section 3a).

It is therefore, concluded that the radiotracer approach is efficient in solving atmospheric deposition in soil, even if the extension of the approach to the whole compositional dataset in order to detect unambiguously atmospherically derived components would require an increase of resolution in soil sampling and associated vertical profile, as performed, for instance, by Landis et al. (2016).

3.c. Organic compounds

Differently from elements and radionuclidic components discussed above, PAHs and paraffins, chosen for their likely atmospheric origin similarly to the airborne radiotracers on which this paper

422 is based, were analyzed in the bulk cores, mixing the whole upper soil 20 cm without sectioning. In
423 this case, no vertical profiles of organics were available, therefore data and correlations were
424 studied considering exclusively inventories of organic pollutants in analogy and association with
425 $^{210}\text{Pb}_{\text{ex}}$ and ^{137}Cs inventories. Total PAH has a high linear coefficient of determination with soil TOC
426 ($R^2 \approx 0.85$), owing to the high affinity with this macro soil component.

427 The comparison of PAH's inventories across the soil transect (Figure 5A) reveals that the bottom
428 stations (LGR, PRI and PCE), all located within the Terni conurbation, present the maximum
429 deposition of these pollutants.

430 In particular, all the three urban stations present PAH concentration values 7 - 45 times higher than
431 the average of all the remaining stations, indicating an extremely high degree of local pollution; in
432 addition PCE presents by far the highest total PAH concentration level together with the highest
433 HMW (high molecular weight) PAH's concentrations, possibly in association again with enhanced
434 aerosol interception by the tree canopy. The highest LMW (Low Molecular Weight) PAH's fraction
435 was detected at LGR, a site more exposed to vehicular traffic. Outside the urban environment, the
436 concentration profile of PAHs along the two sides of the transect, showed a certain degree of
437 increase with height and deposition pattern similar to the radionuclidic inventories with higher
438 depositions on the left branch suggesting the potential for similar depositional behavior with height
439 (see Figure 5B). However, the complex environmental behavior of PAH's ranging from different
440 volatilities as a function of molecular mass to photodegradation and/or nitrification in the
441 troposphere, prevent from conclusive deductions on this class of organic pollutants.

442 Paraffins do not show any clear depositional pattern with height, nor specific trends were found for
443 the carbon preference index - CPI (Lichtfouse, 1995) or low vs. high molecular weight paraffins. This
444 observation is in agreement with the findings of Luo et al. (2012), who attributed a large part of the

445 variance of paraffins in soil samples vs. elevation to vegetation and bacterial processing rather than
446 to atmospheric transport.

447

448 *3.d. Pollutant dispersion in the Terni basin valley: CALPUFF modeling*

449 The atmospheric deposition detected along the soil transect is supported by the output of the
450 CALPUFF dispersion model. The model was run for the full 2014 meteorological year and showed
451 higher cumulate precipitations at the higher elevation sites (Figure 6) which are in reasonably
452 satisfactory agreement with measured total precipitations recorded by the Regional Hydrographic
453 Network (<https://servizioidrografico.regione.umbria.it>, accessed 21/04/2020) reported in Table 3.
454 Measured precipitations show a slight prevalence of the NW stations. We note that the highest
455 depositions of radionuclides and chemical species have been observed on the NW branch of the
456 transect, although relative maxima have also been observed in the SE branch. Since the major
457 mechanism of removal of the accumulation mode (300-700 nm) is wet scavenging, this observation
458 is expected to be in agreement with the pattern of the measured precipitation.

459 The wind roses obtained with the same model runs (Figure 7) show a consistent northerly-
460 northwesterly pattern compatible with an excess accumulation of atmospheric deposition on the
461 north-western branch of the sampling transect, mainly if a seeder-feeder driven phenomenology
462 with mediation by orographic clouds is invoked.

463 The total wet and dry deposition pattern obtained as an outcome of the model is shown in Figure
464 8. Maxima are located in the valley bottom, near the PCE, LGR, and PRI sites, but the TSP extends,
465 consistent with the precipitation pattern, towards the higher elevation areas of the computational
466 grid with a slight prevalence of the Northern sectors.

467 Based on the results from numerical simulations together with the previous pattern of radionuclides
468 and soil composition, we speculate that the plume developing in the Terni bottom airshed enriched

469 in secondary inorganic aerosol, heavy metals, organic pollutants, and radon from which $^{210}\text{Pb}_{\text{ex}}$ is
470 generated, might be uplifted and wet-removed through a seeder-feeder process promoted by the
471 atmospheric circulation. Considering that the CALPUFF modeling is based *de facto* on a single
472 source, the qualitative agreement of the model simulations with the observations along the transect
473 can be considered as a reasonable support of the reasonings herein presented.

474

475 **4. Conclusions**

476 In this paper, we have presented a systematic approach capable of evaluating and describing the
477 deposition process over the Terni district by intercepting the occurrence of the atmospheric
478 components into the soil and atmospheric modelling. The experimental method is based on the
479 use of airborne radionuclides as tracers of atmospheric deposition in a complex mixture of
480 chemical species ranging from inorganic elements to organic molecular species, directly
481 determined in soil profiles. The similarity between soil sampling stations and their association with
482 atmospheric radionuclides is also achieved by means of multivariate statistical analysis.

483 A significant anthropic impact at low altitude across the Terni basin stations has been detected,
484 because of their proximity of residential and industrial sides, with respect to higher altitude
485 stations. This piece of information is evidenced both by the presence of higher concentrations of
486 PAHs, linked to more anthropogenic pollution, and in a more considerable disturbance of the
487 depth profiles of atmospheric radionuclides. The significant role of the planetary boundary layer in
488 trapping pollutants within a shallow mixing height has been already pointed out in other studies
489 conducted in the Terni valley (Ferrero et al., 2012, 2014; Massimi et al. 2019). Herein, we confirm
490 that this is the prevalent atmospheric process that regulates the dispersion of locally generated
491 pollutants in basin valleys. A higher deposition of atmospheric radionuclides has also been

492 assessed in stations at higher altitudes, in particular on the NNW side of the transect. This process
493 is more related to long-range transport of pollutants and enlightens the important role of
494 medium- or high-altitude monitoring sites to study transboundary pollution (Petroselli et al., 2018,
495 2019; Federici et al., 2018; Moroni et al., 2019).

496 The comparison of atmospheric deposition data with the output of a CALPUFF application to the
497 Terni district shows a satisfactory agreement, even though part of the phenomenology that we
498 assume as being related to orographic precipitation, is not sufficiently captured due to the limited
499 model resolution.

500 This work represents a multidisciplinary approach for assessing the atmospheric deposition process
501 into soils, and further studies will be carried out in order to deepen also the soil contamination
502 across the Terni district.

503

504 **Acknowledgements**

505 The authors thank MIUR and Perugia University for financially supporting the research through the
506 AMIS project (“Dipartimenti di Eccellenza-2018-2022”) and Arpa Umbria for collaboration in the
507 CALPUFF dispersion model.

508

509

510 **References**

511 Arpa (Agenzia Regionale per la protezione ambientale) Umbria, 2013. Qualità dell’aria nella
512 provincia di Terni tra il 2002 e il 2011. Available at: [https://www.arpa.umbria.it/pagine/la-qualita-](https://www.arpa.umbria.it/pagine/la-qualita-dellaria-nella-provincia-di-terni-tra-i)
513 [dellaria-nella-provincia-di-terni-tra-i](https://www.arpa.umbria.it/pagine/la-qualita-dellaria-nella-provincia-di-terni-tra-i) , last accessed 21/04/2020, in Italian

514 Baskaran, M. (ed.), 2011. Handbook of Isotope Geochemistry Vol.1, Springer-Verlag Berlin
515 Heidelberg, pp.951.

516 Battiston, G.A., Degetto, S., Gerbasi, R., Sbrignadello, G., Tositti, L., Croatto, U., 1987. The deposition
517 of chernobyl fallout in North-east Italy. *Inorganica Chimica Acta*, 140(C), 327-329.

518 Bettoli, M.G., Cantelli, L., Degetto, S., Tositti, L., Tubertini, O., Valcher, S., 1995. Preliminary
519 investigations on ^7Be as a tracer in the study of environmental processes. *Journal of Radioanalytical*
520 *and Nuclear Chemistry Articles*, 190(1), 137-147.

521 Blackwell B.D., Driscoll, C.T., 2015. Deposition of Mercury in Forests along a Montane Elevation
522 Gradient. *Environmental Science and Technology*, 49, 5363-5370.

523 Brattich, E., Hernández-Ceballos, M.A., Orza, J.A.G., Bolívar, J.P., Tositti, L., 2016. The western
524 Mediterranean basin as an aged aerosols reservoir. Insights from an old-fashioned but efficient
525 radiotracer, *Atmospheric Environment*, 141, 481-493.

526 Brattich E., Hernandez-Ceballos, M.A., Cinelli, G., Tositti, L., 2015a. Analysis of ^{210}Pb peak values at
527 Mt. Cimone (1998-2011), *Atmospheric Environment*, 112, 136-147.

528 Brattich, E., Riccio, A., Tositti, L., Cristofanelli, P., Bonasoni, P., 2015b. An outstanding Saharan dust
529 event at Mt. Cimone (2165 m a.s.l., Italy) in March 2004. *Atmospheric Environment*, 113, 223-235.

530 CALPUFF, 2001. Modeling System Version 6 User Instructions, <http://www.src.com/calpuff/>.

531 Canepari S., Perrino C., Oliviero F., Astolfi M.L., 2008. Characterization of the traffic sources of PM
532 through size-segregated sampling, sequential leaching and ICP analysis. *Atmospheric Environment*
533 42, 8161-8175.

534 Cinelli G., Tositti L., Capaccioni B., Brattich E., Mostacci D., 2014. Soil gas radon assessment and
535 development of a radon risk map in Bolsena, Central Italy. *Environmental Geochemistry and Health*
536 37(2), 305-319.

537 Cartechini, L., Castellini, S., Moroni, B., Palmieri, M., Scardazza, F., Sebastiani, B., Selvaggi, R.,
538 Vagnini, M., Delogu, G.L., Brunetti, B.G., Cappelletti, D., 2015. Acute episodes of black carbon and
539 aerosol contamination in a museum environment: Results of integrated real-time and off-line
540 measurements, *Atmos. Environ.* 116, 130-137.

541 Daly A., P. Zannetti., 2007. Air Pollution Modeling - An Overview. *Ambient air pollution*, 15-28.

542 Federici E., Petroselli C., Montalbani E., Casagrande C., Ceci E., Moroni B., La Porta G., Castellini S.,
543 Selvaggi R., Sebastiani B., Crocchianti S., Gandolfi I., Franzetti A., Cappelletti D., 2018. Airborne
544 bacteria and persistent organic pollutants associated with an intense Saharan dust event in the
545 Central Mediterranean, *Sci. Tot. Environ.*, 645, 401-410.

546 Ferrero, L., Cappelletti, D., Moroni, B., Sangiorgi, G., Perrone, M. G., Crocchianti, S., Bolzacchini, E.,
547 2012. Wintertime aerosol dynamics and chemical composition across the mixing layer over basin
548 valleys, *Atmos. Environ.*, 56, 143-153, doi:10.1016/j.atmosenv.2012.03.071

549 Ferrero, L., Castelli, M., Ferrini, B.S., Moscatelli, M., Perrone, M.G., Sangiorgi, G., Rovelli, G.,
550 D'Angelo, L., Moroni, B., Scardazza, F., Mocnik, G., Bolzacchini, E., Petitta, M., Cappelletti, D., 2014.
551 Impact of Black Carbon Aerosol over Italian basin valleys: high resolution measurements along
552 vertical profiles, radiative forcing and heating rate. *Atmos. Chem. Phys.*, 14, 9641-9664.

553 Fowler D., Cape, J. N., Leith, I. D. Choularton, T. W. Gay, M. J., Jones, A. 1988. The influence of
554 altitude on rainfall composition at Great Dun Fell. *Atmospheric Environment*, 22(7), 1355-1362.

555 Fowler, D., Mourné, R., Branford, D., 1995. The application of ^{210}Pb inventories in soil to measure
556 long-term average wet deposition of pollutants in complex terrain, *Water, Air and Soil Pollution*, 85,
557 2113-2118.

558 Fowler, D., Skiba, U., Nemitz, E., Choubedar, F., Branford, D., Donovan, R., Rowland, P., 2004.
559 Measuring aerosol and heavy metal deposition on urban woodland and grass using inventories of
560 ^{210}Pb and metal concentrations in soil. *Water, Air and Soil Pollution Focus* 4, 483-499.

561 Franzini M., Leoni L., Saitta M., 1972. A simple method to evaluate the matrix effects in X-ray
562 fluorescence analysis. *X-Ray Spectrometry* 1, 151-154.

563 Franzini M., Leoni L., Saitta M., 1975. Revisione di una metodologia analitica per fluorescenza-X
564 basata sulla correzione completa degli effetti di matrice. *Rendiconti della Società Italiana di*
565 *Mineralogia e Petrologia* 31, 365-378.

566 Gabriel K. R., 1971. The biplot graphic display of matrices with application to principal component
567 analysis. *Biometrika*, 58(3), 453-467.

568 Gelencsér A., 2004. Carbonaceous aerosol: atmospheric and oceanographic sciences library.
569 Springer Publications, Dordrecht, the Netherlands, 184-190.

570 Gilmore G.R., 2008. Practical Gamma-Ray Spectrometry, 2nd Edition. John Wiley & Sons, Ltd.

571 Gogou A., Stratigakis N., Kanakidou M., and Stephanou E.G., 1996. Organic aerosols in eastern
572 Mediterranean: components source reconciliation by using molecular markers and atmospheric
573 back trajectories. *Org. Geochem.* 25, 79-96, doi:10.1016/S0146-6380(96)00105-2

574 Graustein, W.C., Turekian, K.K., 1986 ^{210}Pb and ^{137}Cs in air and soils measure the rate and vertical
575 profile of aerosol scavenging, *Journal of Geophysical Research*, 91D, 14355-14366.

576 Graustein, W.C., Turekian, K.K., 1989. The effects of forests and topography on the deposition of
577 sub-micrometer aerosols measured by lead-210 and cesium-137 in soils. *Agricultural and Forest*
578 *Meteorology*, 47(2-4), 199-220.

579 Janoušek V., Farrow C.M., and Erban V., 2006. Interpretation of whole-rock geochemical data in
580 igneous geochemistry: introducing Geochemical Data Toolkit (GCDkit). *Journal of Petrology* 47(6),
581 1255-1259.

582 Jolliffe, I. T., & Cadima, J., 2016. Principal component analysis: a review and recent developments.
583 *Philosophical Transactions of the Royal Society A: Mathematical, Physical and Engineering Sciences*,
584 374(2065), 20150202.

585 Jongen, S., Bonafe, G., 2006. LAMI Verification for Air Quality Forecast and Assessment Purposes.
586 Internal report ARPAE-SIM.
587 https://www.arpae.it/smr/archivio/downloads/ambiente/report_lm_verif_fv.pdf
588

589 IAEA, Environmental consequences of the Chernobyl accident and their remediation : twenty years of
590 experience / report of the Chernobyl Forum Expert Group 'Environment'. — Vienna : International Atomic
591 Energy Agency, 2006
592

593 Kaste J.M., Friedland A.J., Stürup S., 2003. Using stable and radioactive isotopes to trace
 594 atmospherically deposited Pb in montane forest soils. *Environ Sci Technol*, 37, 3560-3567.

595 Lamborg C.H., Fitzgerald W.F., Graustein W.C., Turekian K.K., 2000. An examination of the
 596 atmospheric chemistry of mercury using ^{210}Pb and ^7Be . *Journal of Atmospheric Chemistry* 35, 325-
 597 338.

598 Lancianese V., Dinelli E., 2016. Geochemical mapping based on geological units: a case study from
 599 the Marnoso-arenacea formation (Northern Apennines, Italy). *Chemie der Erde – Geochemistry*
 600 76(1), 49-62, doi:10.1016/j.chemer.2015.12.001

601 Landis, J. D., Renshaw, C. E., Kaste, J. M., 2014. Quantitative Retention of Atmospherically Deposited
 602 Elements by Native Vegetation Is Traced by the Fallout Radionuclides ^7Be and ^{210}Pb . *Environmental*
 603 *Science and Technology*, 48(20), 12022-12030.

604 Landis, J.D., Renshaw, C.E., Kaste J.M, 2016. Beryllium-7 and Lead-210 chronometry of modern soil
 605 processes: the Linked Radionuclide ACcumulation model (LCA), *Geochimica et Cosmochimica Acta*,
 606 180, 109-125

607 Le Roux, G., Pourcelot, L., Masson, O., Duffa, C., Vray, F., Renaud, P., 2008. Aerosol deposition and
 608 origin in French mountains estimated with soil inventories of ^{210}Pb and artificial radionuclides,
 609 *Atmospheric Environment*, 42 (7), 1517-1524.

610 Lichtfouse, E., Eglinton, T. I. (1995). ^{13}C and ^{14}C evidence of pollution of a soil by fossil fuel and
 611 reconstruction of the composition of the pollutant. *Organic Geochemistry*, 23(10), 969-973.

612 Likuku A.S., Branford D., Fowler D., Weston K.J., 2006. Inventories of fallout ^{210}Pb and ^{137}Cs
 613 radionuclides in moorland and woodland soils around Edinburgh urban area (UK). *Journal of*
 614 *Environmental Radioactivity*, 90 (1), 37-47.

615 Likuku A.S., 2006. Wet deposition of ^{210}Pb aerosols over two areas of contrasting topography,
 616 *Environ. Res. Lett.* 1,1, 014007.

617 Luo P., Peng P.A., Lü H.Y., Zheng Z., Wang X., 2012. Latitudinal variations of CPI values of long-chain
618 n-alkanes in surface soils: Evidence for CPI as a proxy of aridity. *Sci China Earth Sci*, 55, 1134-1146,
619 doi: 10.1007/s11430-012-4401-8

620 Mabit, L., Benmansour, M., Abril, J.M., Walling, D.E., Meusburger, K., Iurian, A.R., Bernard, C., Tarján,
621 S., Owens, P.N., Blake, W.H., Alewell, C., 2014. Fallout ²¹⁰Pb as a soil and sediment tracer in
622 catchment sediment budget investigations: A review, *Earth-Science Reviews*, 138, 335-351

623 Massimi L., Conti M.E., Mele G., Ristorini M., Astolfi M.L., Canepari S., (2019) Lichen transplants as
624 indicators of atmospheric element concentrations: a high spatial resolution comparison with PM₁₀
625 samples in a polluted area (Central Italy), *Ecological Indicators*, 101, 759-769.

626 Masson, O., Baeza, A., Bieringer, J., Brudecki, K., Bucci, S., Cappai, M., Carvalho, F.P., Connan, O.,
627 Cosma, C., Dalheimer, A., Didier, D., Depuydt, G., De Geer, L.E. De Vismes, A., Gini, L., Groppi, F.,
628 Gudnason, K. Gurriaran, R., Hainz, D., Halldórsson, Ó, Hammond, D., Hanley, O., Holeý, K., Homoki,
629 Zs., Ioannidou, A., Isajenko, K., Jankovic; C. Katzlberger; M. Kettunen; R. Kierepko; R. Kontro; P.J.M.
630 Kwakman; M. Lecomte, M. Leon Vintro, L., Leppänen, A.-P., Lind, B., Lujaniene, G., Mc Ginnity, G.,
631 Mc Mahon, C., Malá, C., Manenti, S., Manolopoulou, M., Mattila, A., Mauring, A., Mietelski, J.W.,
632 Møller, B., Nielsen, S.P., Nikoli κ, J., Overwater, R.M.W., Pálsson, S. E., Papastefanou, A., Penev, I.,
633 Pham, M.K., Povinec, P.P., Ramebäck, H., Reis, M.C., Ringer, W., Rodriguez, A., Rulík, P., Saey, P.R.J.,
634 Samsonov, V., Shlosser, C., Sgorbati, G., Silobritiene, B. V., Söderström, C., Sogni, R., Solier, L., Sonk,
635 M., Steinhäuser, G., Steinkopff, T., Steinmann, P., Stoulos, S., Sýkora, I., Todorovic, D., Tooloutalaie,
636 N., Tositti, L., Tshiersh, J., Ugron, A., Vagena, E., Vargas, A., Wershofen, H., and Zhukova, O., 2011.
637 Tracking of Airborne Radionuclides from the Damaged Fukushima Dai-Ichi Nuclear Reactors by
638 European Networks, *Environmental Science and Technology* 45, 7670-7677

639 Meloni D., Carpine F., 2004. Cinquanta anni (1953-2002) di osservazioni meteo a Terni. Ed: Provincia
640 di Terni, pp 79.

641 Moroni, B., Cappelletti, D., Marmottini, F., Scardazza, F., Ferrero, L., Bolzacchini, E., 2012. Integrated
642 single particle-bulk chemical approach for the characterization of local and long range sources of
643 particulate pollutants. *Atmos. Environ.* 50, 267–277.

644 Moroni B., Ferrero L., Crocchianti S., Perrone M.G., Sangiorgi G., Bolzacchini E., Cappelletti D., 2013.
 645 Aerosol dynamics upon Terni basin (Central Italy): results of integrated vertical profile
 646 measurements and electron microscopy analyses. *Rendiconti Lincei* 24, 319-328.

647 Moroni B., Castellini S., Crocchianti S., Piazzalunga A., Fermo P., Scardazza F., Cappelletti D., 2015.
 648 Ground-based measurements of long-range transported aerosol at the rural regional background
 649 site of Monte Martano (central Italy). *Atmospheric Research* 155, 26-36,

650 Moroni B., Crocchianti S., Petroselli C., Selvaggi R., Becagli S., Traversi R., Cappelletti D., 2019.
 651 Potential source contribution function analysis of long-range transported aerosols in the Central
 652 Mediterranean: a comparative study of two background sites in Italy, *Rend. Fis. Acc. Lincei*, 30, 337-
 653 349.

654 Núñez-Alonso, D., Pérez-Arribas, L.V., Manzoor, S., Cáceres, J.O., 2019. Statistical Tools for Air
 655 Pollution Assessment: Multivariate and Spatial Analysis Studies in the Madrid Region. *Journal of*
 656 *analytical methods in chemistry*, 2019, 9753927. doi:10.1155/2019/9753927

657 ORTEC, 2003. Gamma-Vision 32 A66-B32 User's manual. ORTEC USA, Part. No. 783620 Manual
 658 Revision D.

659 Perez-Bendito D. and Rubio S., Chapter 14 Chemometrics in environmental analysis.
 660 (1999). *Environmental Analytical Chemistry*, 747–833. doi:10.1016/s0166-526x(99)80016-6

661 Persson B.R.R., Holm E., 2011. Polonium-210 and lead-210 in the terrestrial environment: a
 662 historical review, *Journal of Environmental Radioactivity*, 102(5), 420-429.

663 Petroselli C., Crocchianti S., Moroni B., Castellini S., Selvaggi R., Nava S., Calzolari G., Lucarelli F.,
 664 Cappelletti D., 2018. Disentangling the major source areas for an intense aerosol advection in the
 665 Central Mediterranean on the basis of Potential Source Contribution Function modeling of chemical
 666 and size distribution measurements, *Atmospheric Research*, Volume 204, 67-77.

667 Petroselli, C., Moroni, B., Crocchianti, S., Selvaggi, R., Vivani, R., Soggia, F., Grotti, M., D'Acapito, F.,
 668 Cappelletti, D., 2019. Iron Speciation of Natural and Anthropogenic Dust by Spectroscopic and
 669 Chemical Methods. *Atmosphere*, 10(1), 8.

670 Preiss, N., Mélières, M.-A., Pourchet, M., 1996. A compilation of data on lead 210 concentration in
671 surface air and fluxes at the air-surface and water-sediment interfaces. *Journal of Geophysical*
672 *Research: Atmospheres*, 101(D22), 28847-28862.

673 Stankwitz C., Kaste J.M., Friedland A.J., 2012. Threshold increases in soil lead and mercury from
674 tropospheric deposition across an elevational gradient. *Environ Sci Technol* 46, 8061-8068.

675 Suchara I., Sucharova J., Hola M., Pilatova H., Rulik P., 2016. Long-term retention of ¹³⁷Cs in three
676 forest soils with different soil properties. *Journal of Environmental Radioactivity*, 158-159, 102-113.

677 Swarzenski P.W., 2014. ²¹⁰Pb Dating in *Encyclopedia of Scientific Dating Methods*, Springer
678 Science+Business Media Dordrecht.

679 Tositti L., Mingozi M., Sandrini S., Buoso, S., De Poli, M., Ceccato, D., Zafiropoulos, D., 2006. A
680 multitracer study on peat profiles from Tunguska, Siberia. *Global and planetary change*, 53, 278-
681 289.

682 Tositti L., Brattich, E., Cinelli, G., Previti, A., Mostacci, D., 2012. Comparison of radioactivity data
683 measured in PM10 aerosol samples at two elevated stations in northern Italy during the Fukushima
684 event, *Journal of Environmental Radioactivity*, 114, 105–112

685 Tositti, L., Brattich E., Cinelli, G., Baldacci, D., 2014a. 12 years of ⁷Be and ²¹⁰Pb in Mt. Cimone, and
686 their correlation with meteorological parameters, «*Atmospheric Environment*, 87, 108-122.

687 Tositti, L., Brattich, E., Masiol, M., Baldacci, D., Ceccato, D., Parmeggiani, S., Stracquadanio, M.,
688 Zappoli, S., 2014b. Source apportionment of particulate matter in a large city of southeastern Po
689 Valley (Bologna, Italy). *Environmental Science and Pollution Research International*, 21, 872-890.

690 Tositti L., Cinelli G., Brattich E., Galgaro A., Mostacci D., Mazzoli C., Massironi M., Sassi R., 2016.
691 Assessment of lithogenic radioactivity in the Euganean Hills magmatic district (NE Italy). *Journal of*
692 *Environmental Radioactivity*, 166(2), 259-269.

693 Tositti, L., Brattich, E., Parmeggiani, S., Bolelli, L., Ferri, E., Girotti, S., 2018. Airborne particulate
694 matter biotoxicity estimated by chemometric analysis on bacterial luminescence data. *Science of*
695 *the Total Environment*, 640-641, 1512-1520.

696 Turekian, K. K., Nozaki, Y., & Benninger, L. K., 1977. Geochemistry of Atmospheric Radon and Radon
697 Products. *Annual Review of Earth and Planetary Sciences*, 5(1), 227–255.

698 USEPA, 2005. Revision to the Guideline on Air Quality Models: Adoption of a Preferred Long Range
699 Transport Model and Other Revisions; Final Rule, 40 CFR Part 51, Federal Register / Vol. 70, No. 216
700 / Wednesday, November 9, 2005 / Rules and Regulations, 68218;);
701

702 USEPA, 2017. Revision to the Guideline on Air Quality Models: Adoption of a Preferred Long Range
703 Transport Model and Other Revisions; Final Rule, 40 CFR Part 51, Federal Register / Vol. 82, No. 10
704 / January 17, 2017 / Rules and Regulations, 5182;
705

706 van den Berg, R. A., Hoefsloot, H. C., Westerhuis, J. A., Smilde, A. K., & van der Werf, M. J., 2006.
707 Centering, scaling, and transformations: improving the biological information content of
708 metabolomics data. *BMC genomics*, 7(1), 142.
709

710 Vet R., Artz, R.S., Carou, S., Shaw, M., Ro, C.-H, Aas, W., Baker, A., Bowersox, V.C., Dentener, F., Galy-
711 Lacaus, C., Hou, A., Pienaar, J.J., Gillett, R., Forti, M.C., Gromov, S., Hara, H., Khodzher, T., Mahowald,
712 N.M., Nickovic, S., Rao, P.S.P., Reid, N.W., 2014a. A global assessment of precipitation chemistry
713 and deposition of sulfur, nitrogen, sea salt, base cations, organic acids, acidity and pH, and
714 phosphorus, *Atmospheric Environment*, 93, 3-100

715 Vet R., Artz, R.S., Carou, S., Shaw, M., Ro, C.-H, Aas, W., Baker, A., Bowersox, V.C., Dentener, F., Galy-
716 Lacaus, C., Hou, A., Pienaar, J.J., Gillett, R., Forti, M.C., Gromov, S., Hara, H., Khodzher, T., Mahowald,
717 N.M., Nickovic, S., Rao, P.S.P., Reid, N.W., 2014b. Addendum to: “A global assessment of
718 precipitation chemistry and deposition of sulfur, nitrogen, sea salt, base cations, organic acids,
719 acidity and pH, and phosphorus”, *Atmospheric Environment*, 93, 2014, 101-116

720 Westgate, J.N., Wania, F., 2013. Model-based exploration of the drivers of mountain cold-trapping
721 in soil, *Environmental Science Processes Impacts*, 15, 2220

722 Zhang, L., Vet, R., 2006. A review of current knowledge concerning size-dependent aerosol removal,
723 China Particuology, 4, Issue 6, 272-282

724

725

726 **Figure Legends**

727

728 **Figure 1** – Map of the Terni district depicting topography and name/location of the sampling stations
729 occupied in this work. The color scale depicts the altitude (meters above sea level)

730 **Figure 2** - Vertical profiles of $^{210}\text{Pb}_{\text{ex}}$ and ^{137}Cs along the soil sampling transect. The experimental
731 errors associated with each radionuclide data are defined as error bars. Layer depth ranges in cm

732 **Figure 3.** ^{137}Cs and $^{210}\text{Pb}_{\text{ex}}$ inventories (expressed in Bq m^{-2}) in the investigated sites as a function of
733 relative distance and altitude from Terni (both expressed in m). The size of the circles is proportional
734 to the flux, with scales reported to the left of the figure

735 **Figure 4.** Gabriel biplot of Principal Component Analysis (PCA) with $^{210}\text{Pb}_{\text{ex}}$ and ^{137}Cs , PC1 vs. PC2
736 and PC1 vs. PC3

737 **Figure 5.** Total PAH inventory (expressed in mg m^{-2}) as a function of altitude from Terni (expressed
738 in m) for all the investigated sites (A) and excluding the three bottom stations in Terni area (B)

739 **Figure 6.** Cumulated precipitations

740 **Figure 7.** Wind roses for the north-western branch (A) and for the Eastern branch (B)

741 **Figure 8.** Wet and dry deposition as obtained by the CALPUF model (see text)

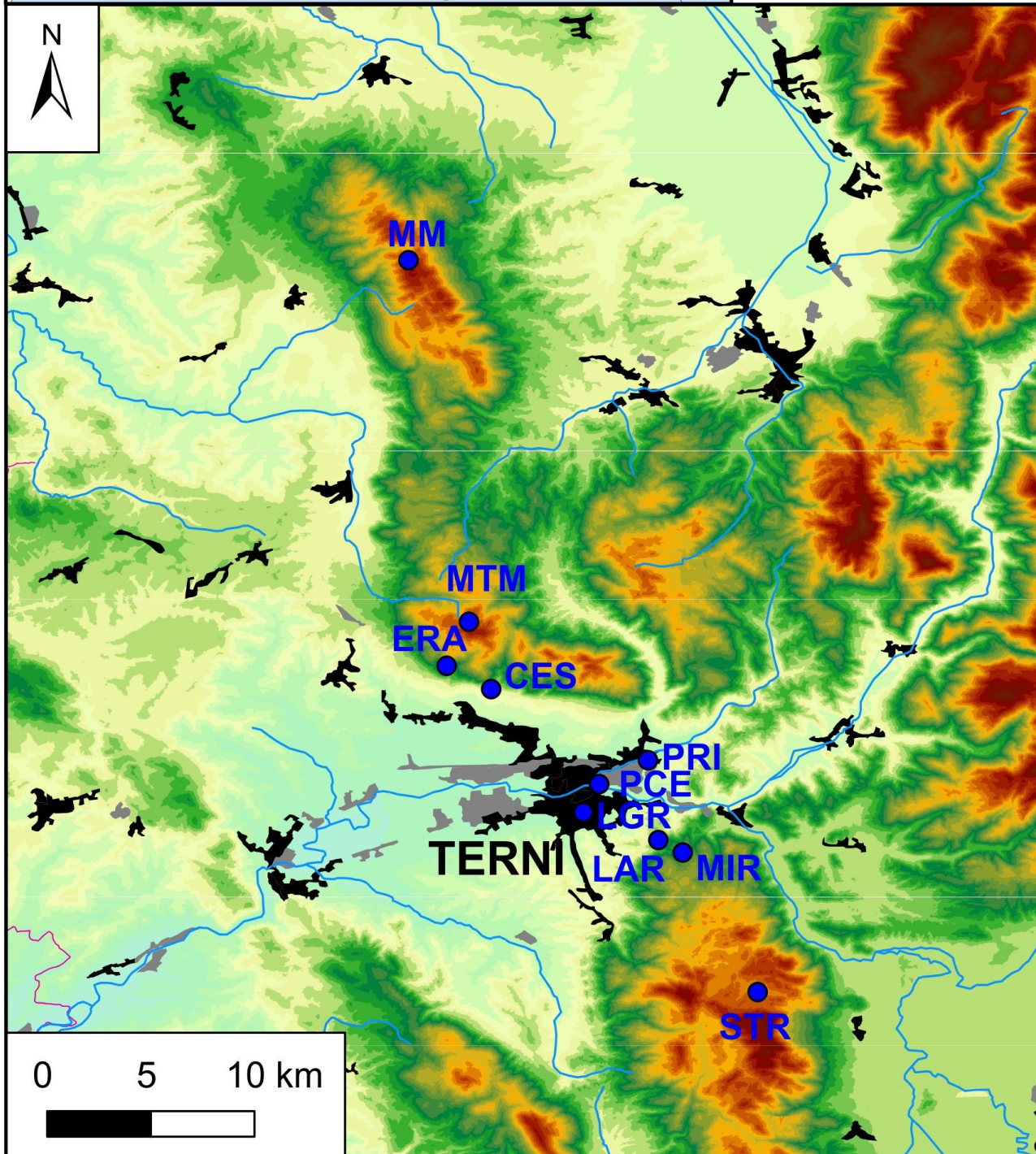
742



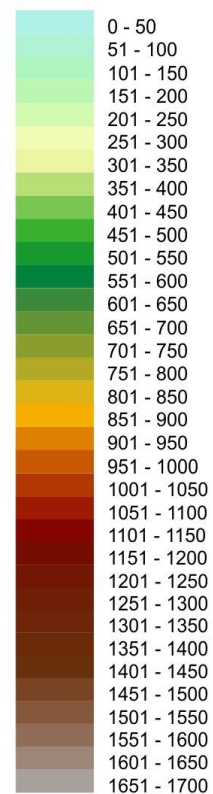
● sampling sites

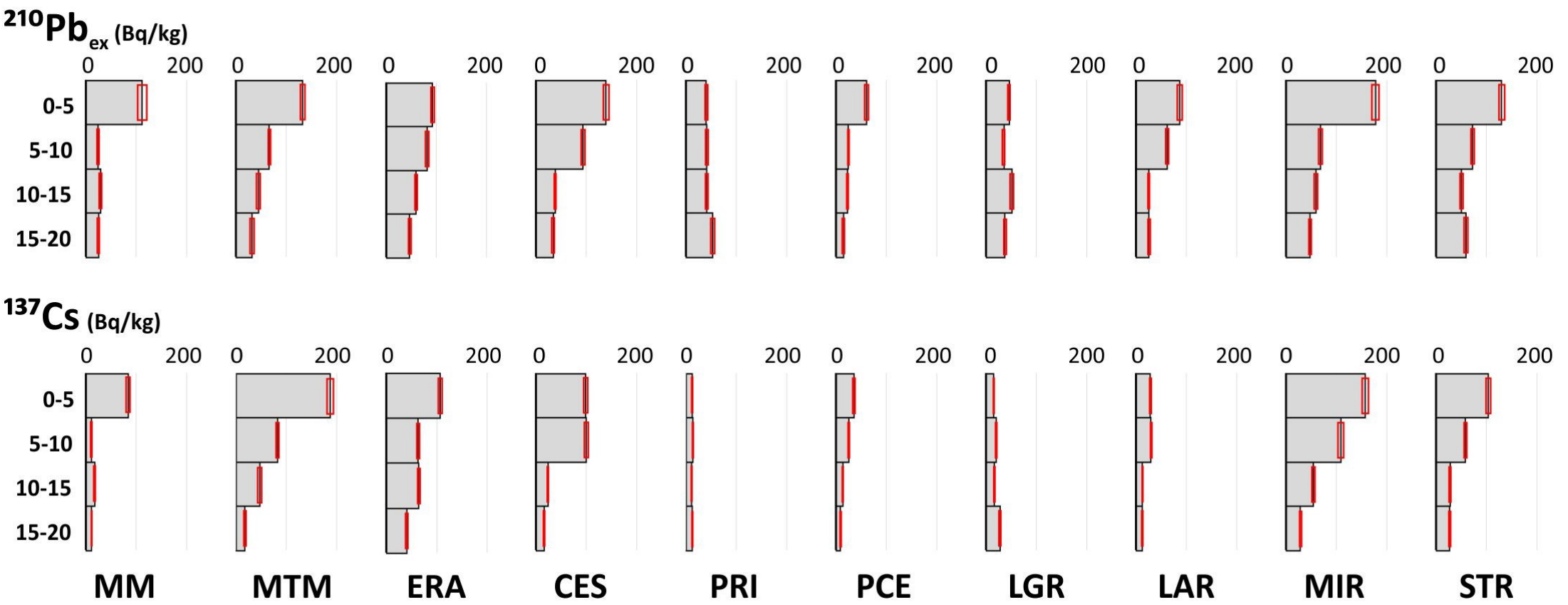
■ Industrial areas

■ Urban areas

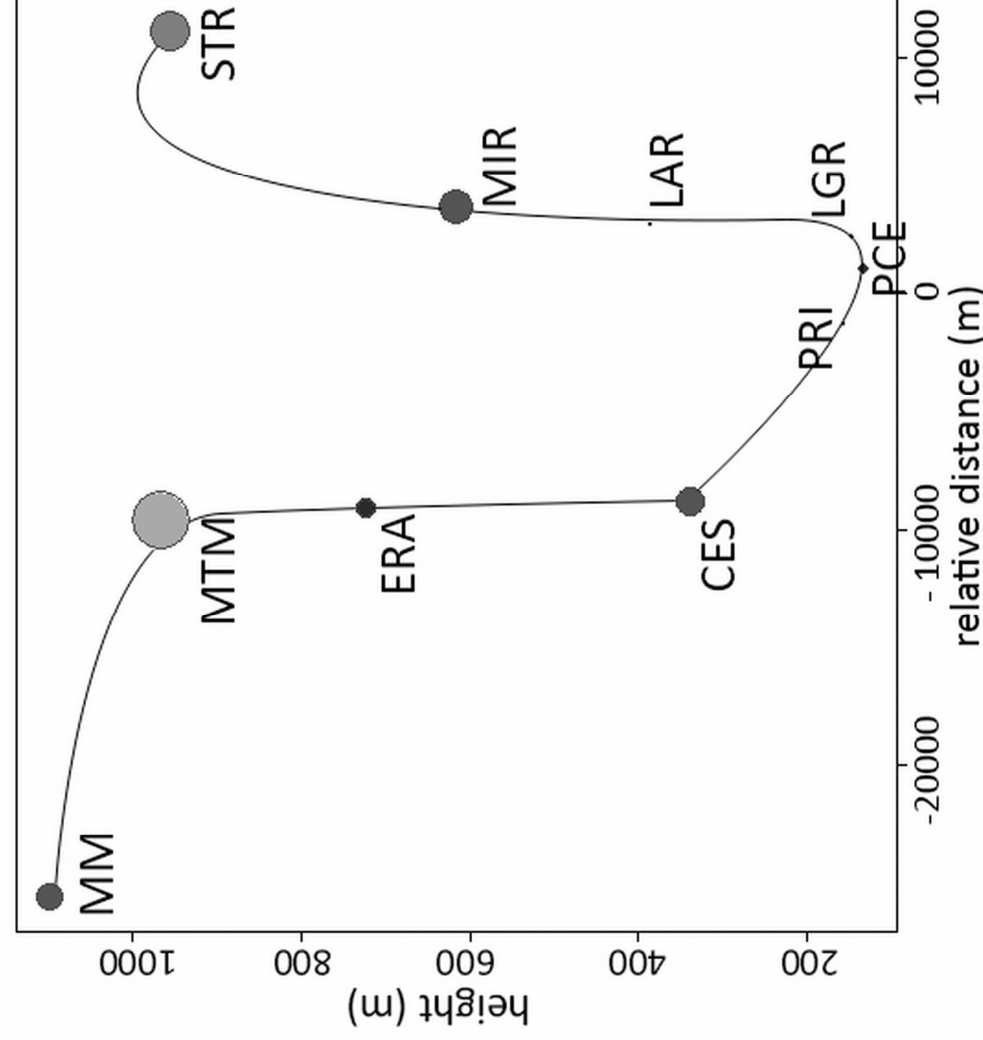
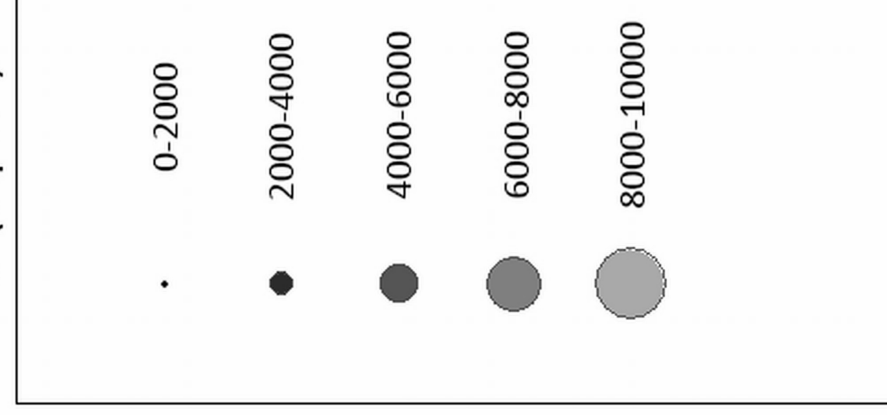


Height above sea level (m)

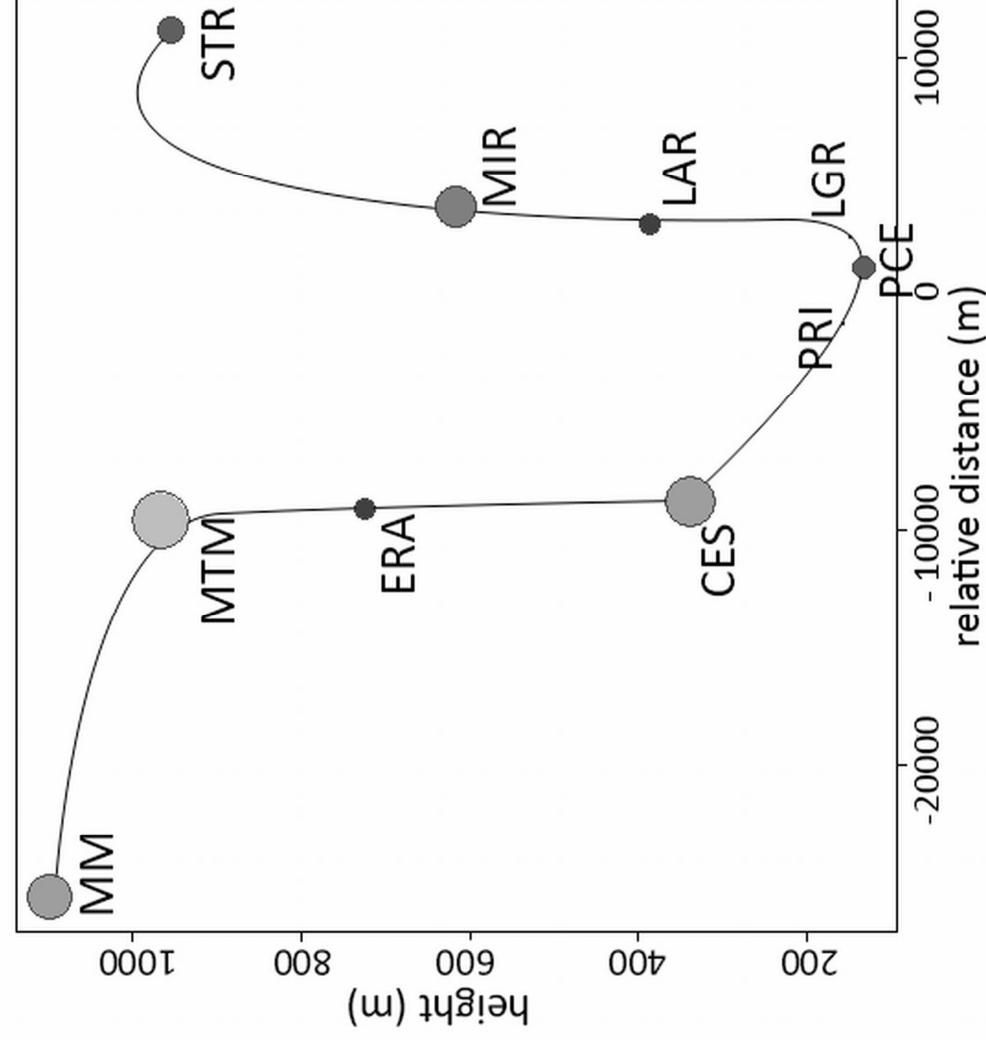
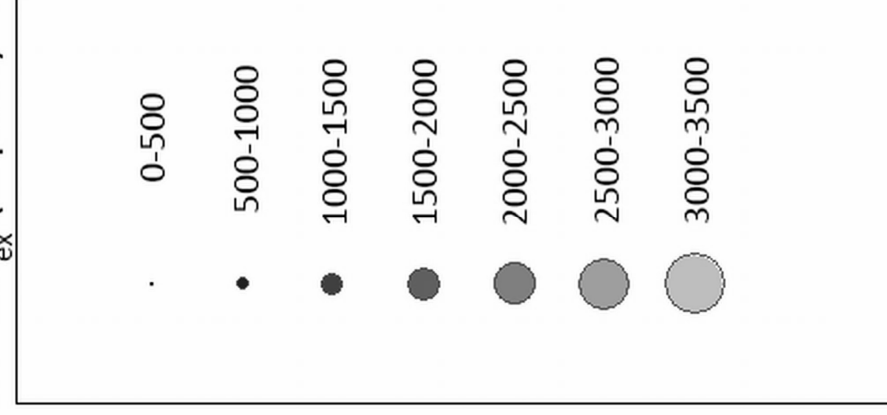


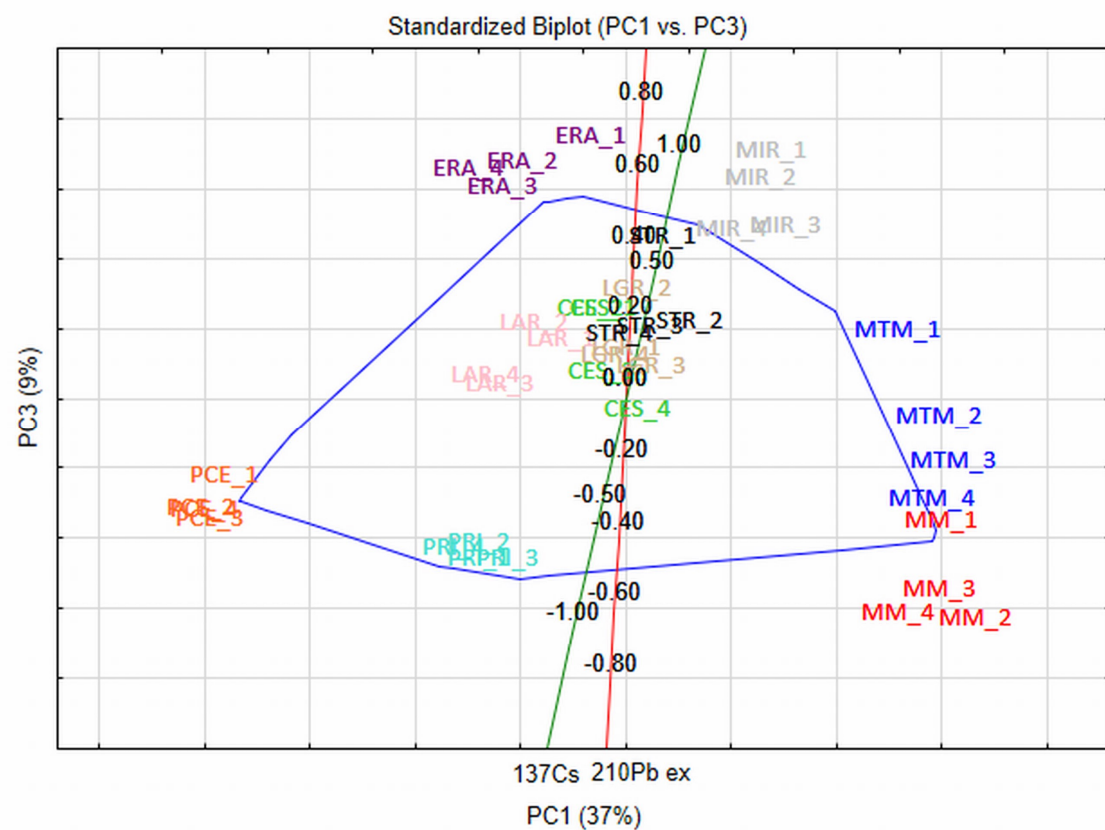
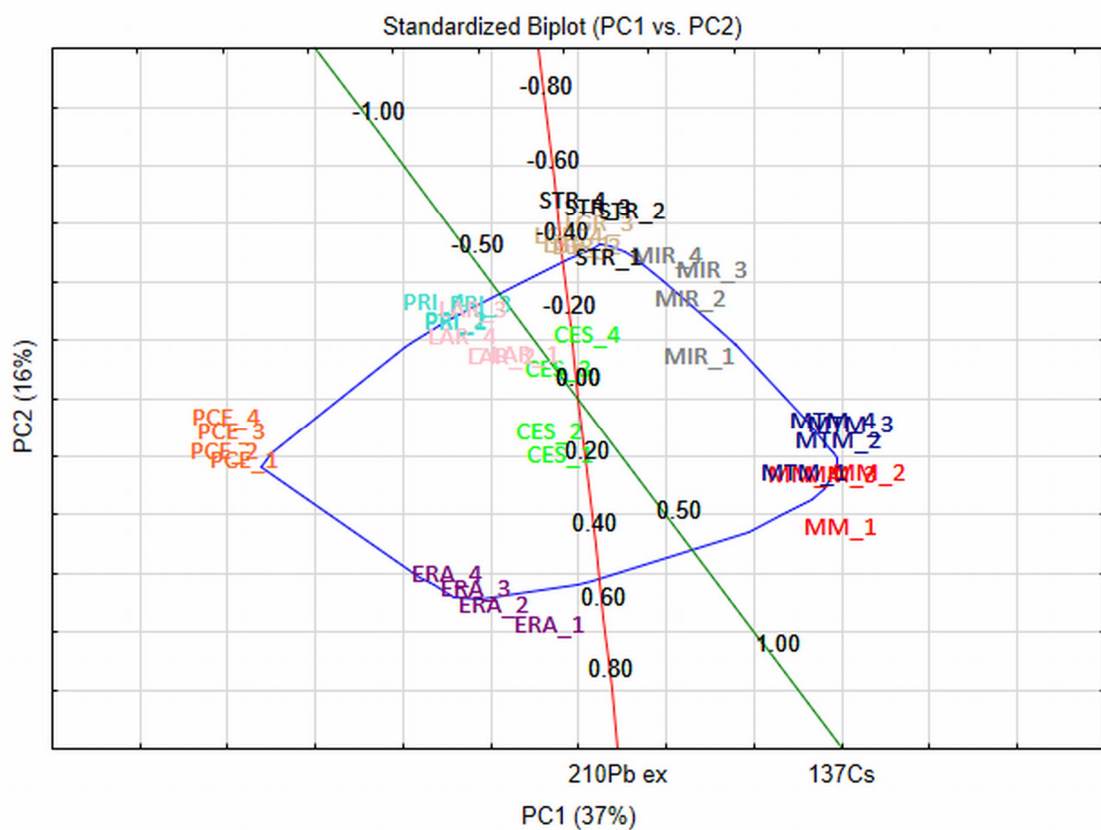


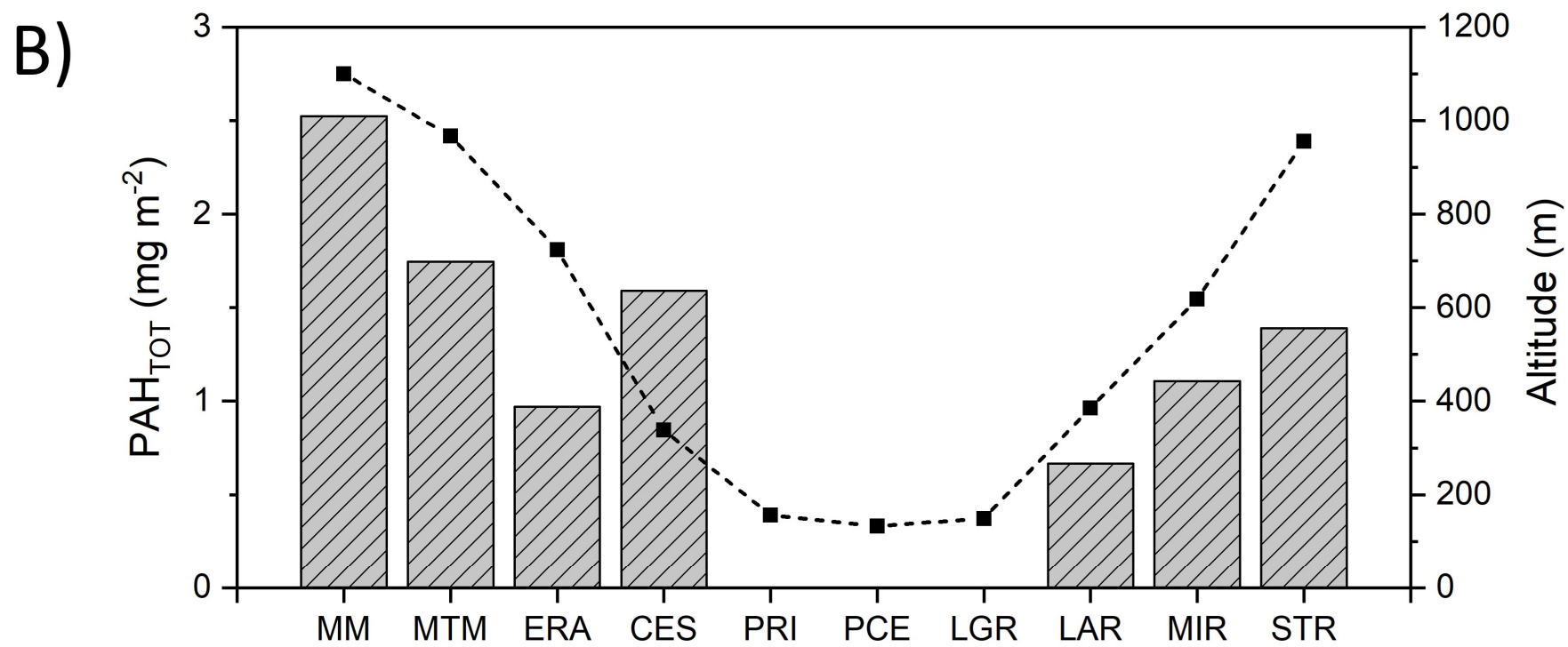
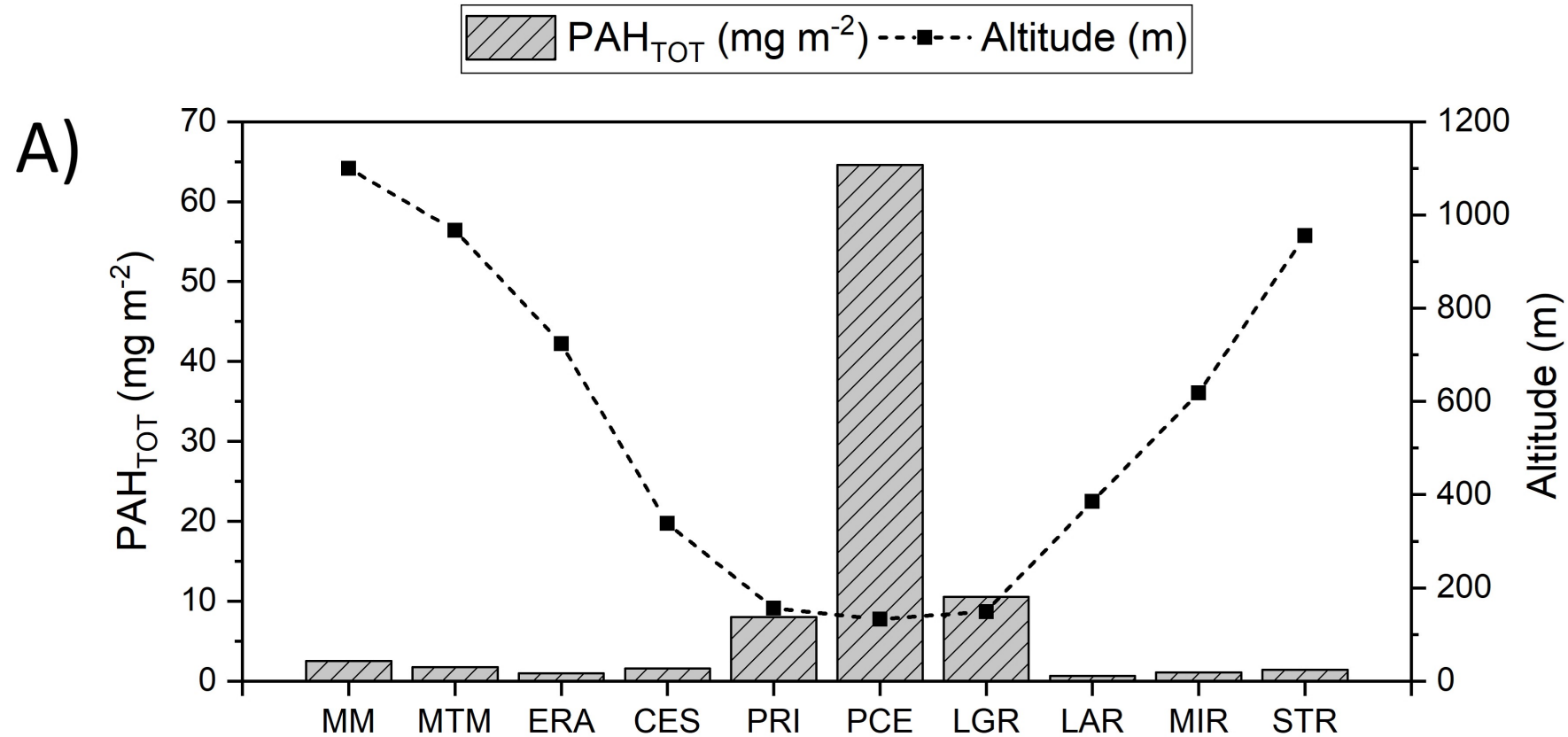
^{137}Cs (Bq m^{-2})

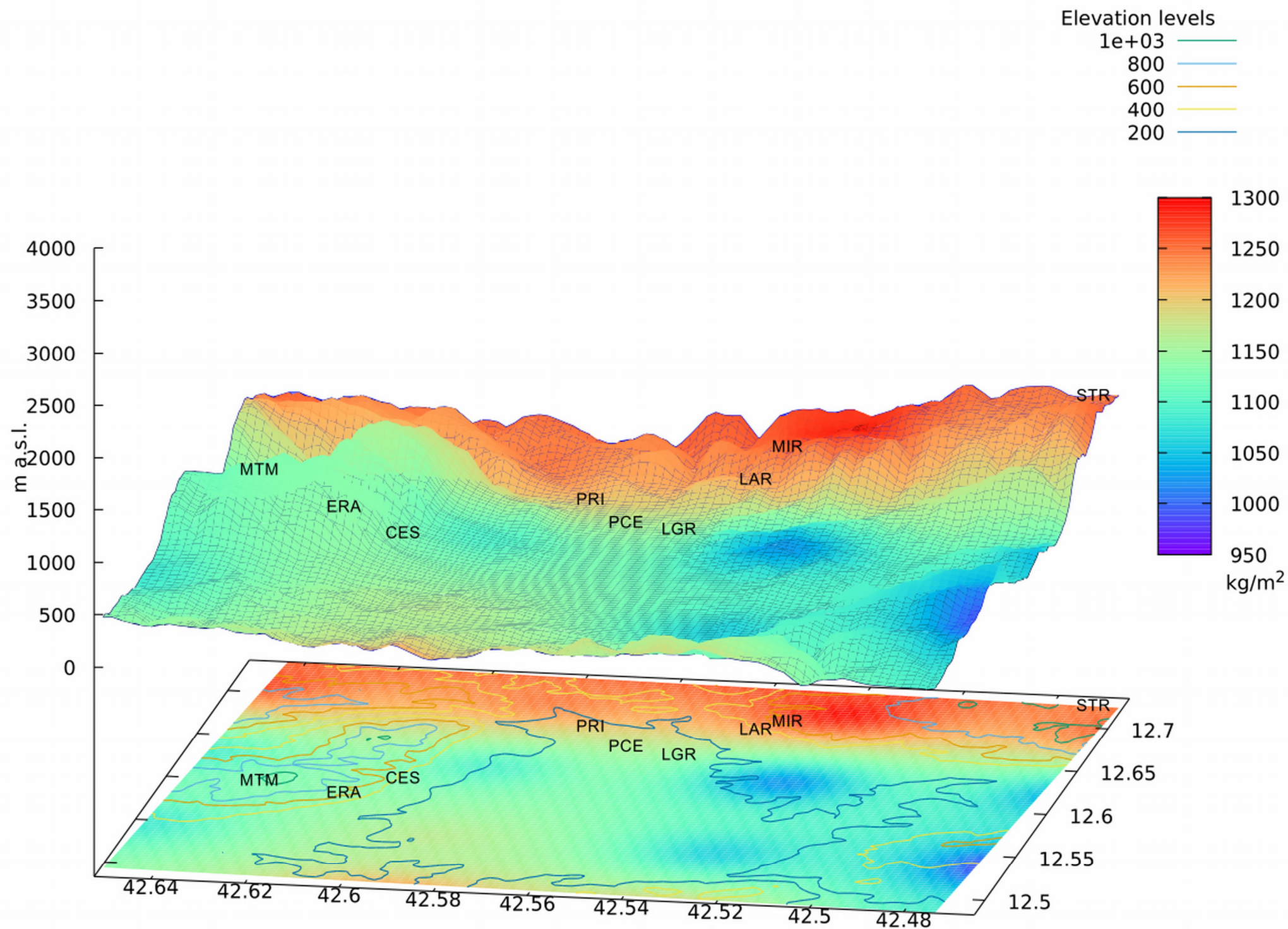


$^{210}\text{Pb}_{\text{ex}}$ (Bq m^{-2})

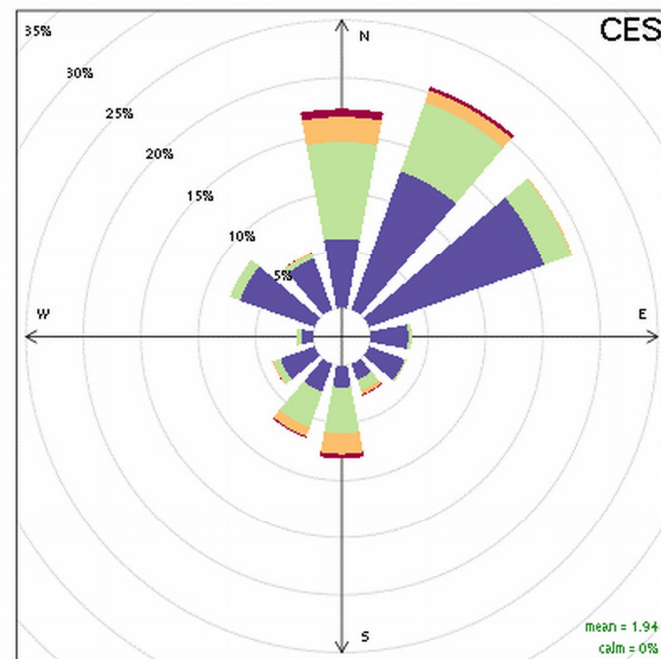
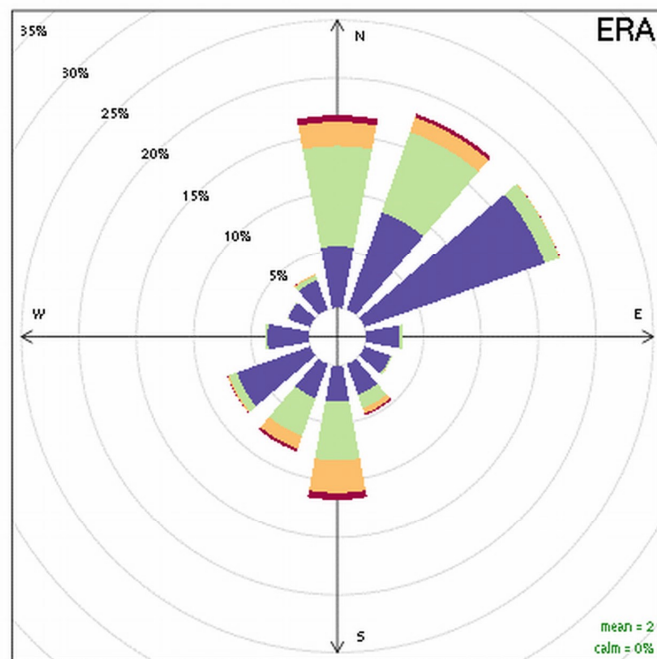
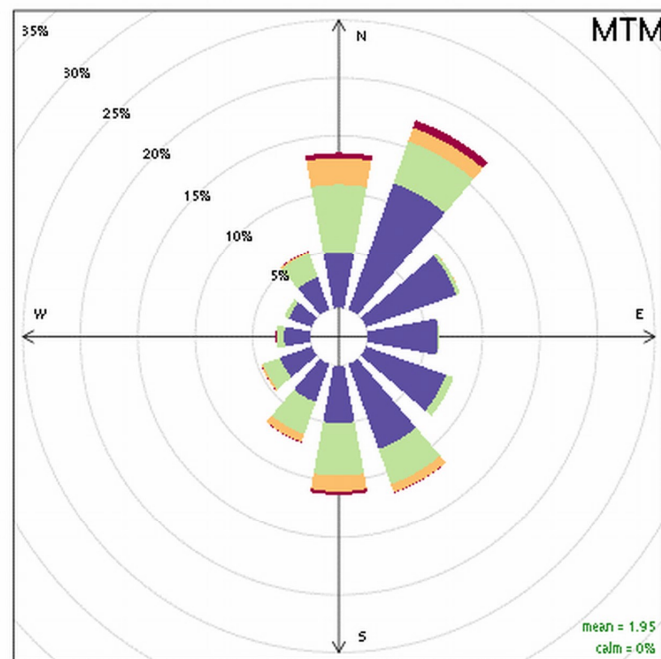








A)

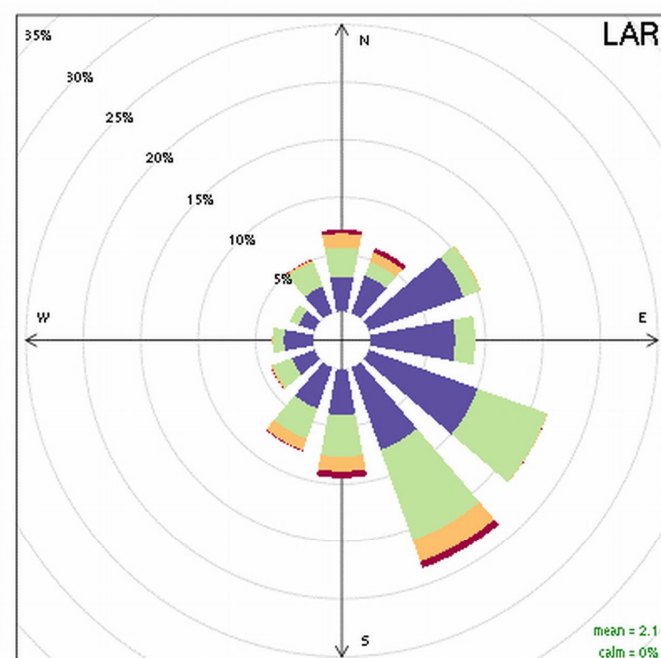
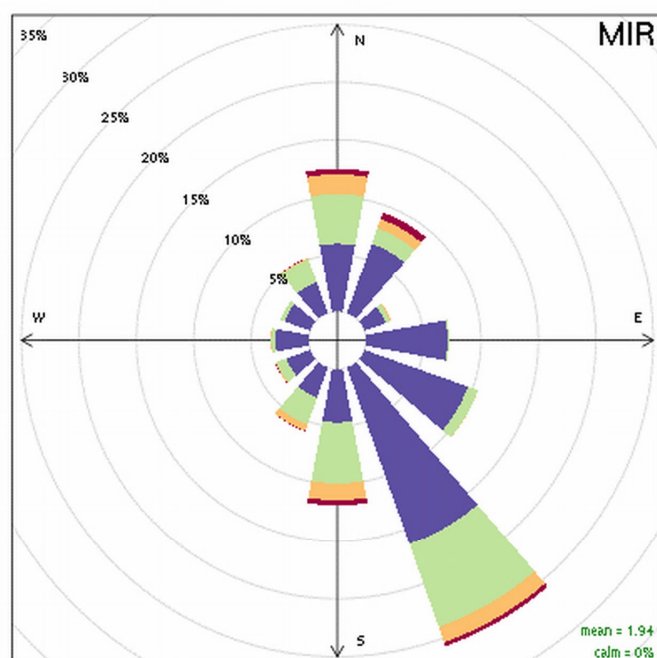
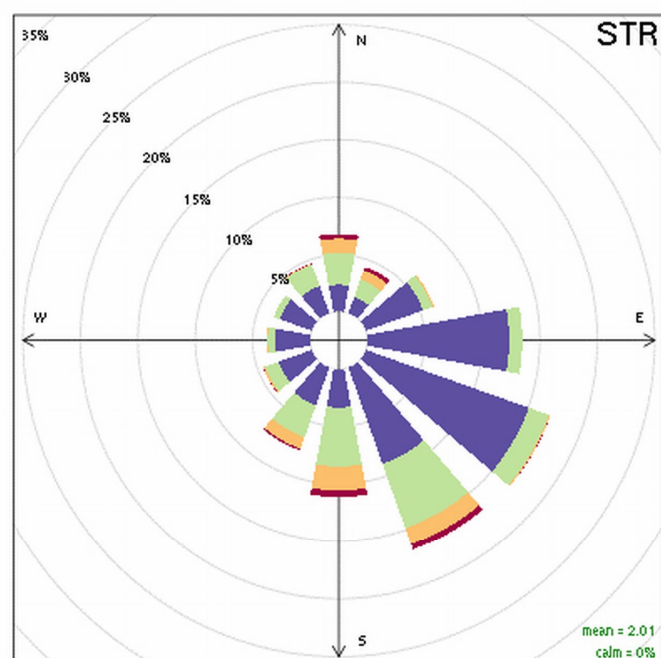


0 to 2 2 to 4 4 to 6 6 to 9.2049
(m s^{-1})
Frequency of counts by wind direction (%)

0 to 2 2 to 4 4 to 6 6 to 9.0861
(m s^{-1})
Frequency of counts by wind direction (%)

0 to 2 2 to 4 4 to 6 6 to 9.1546
(m s^{-1})
Frequency of counts by wind direction (%)

B)



0 to 2 2 to 4 4 to 6 6 to 9.2739
(m s^{-1})
Frequency of counts by wind direction (%)

0 to 2 2 to 4 4 to 6 6 to 9.124
(m s^{-1})
Frequency of counts by wind direction (%)

0 to 2 2 to 4 4 to 6 6 to 9.5905
(m s^{-1})
Frequency of counts by wind direction (%)

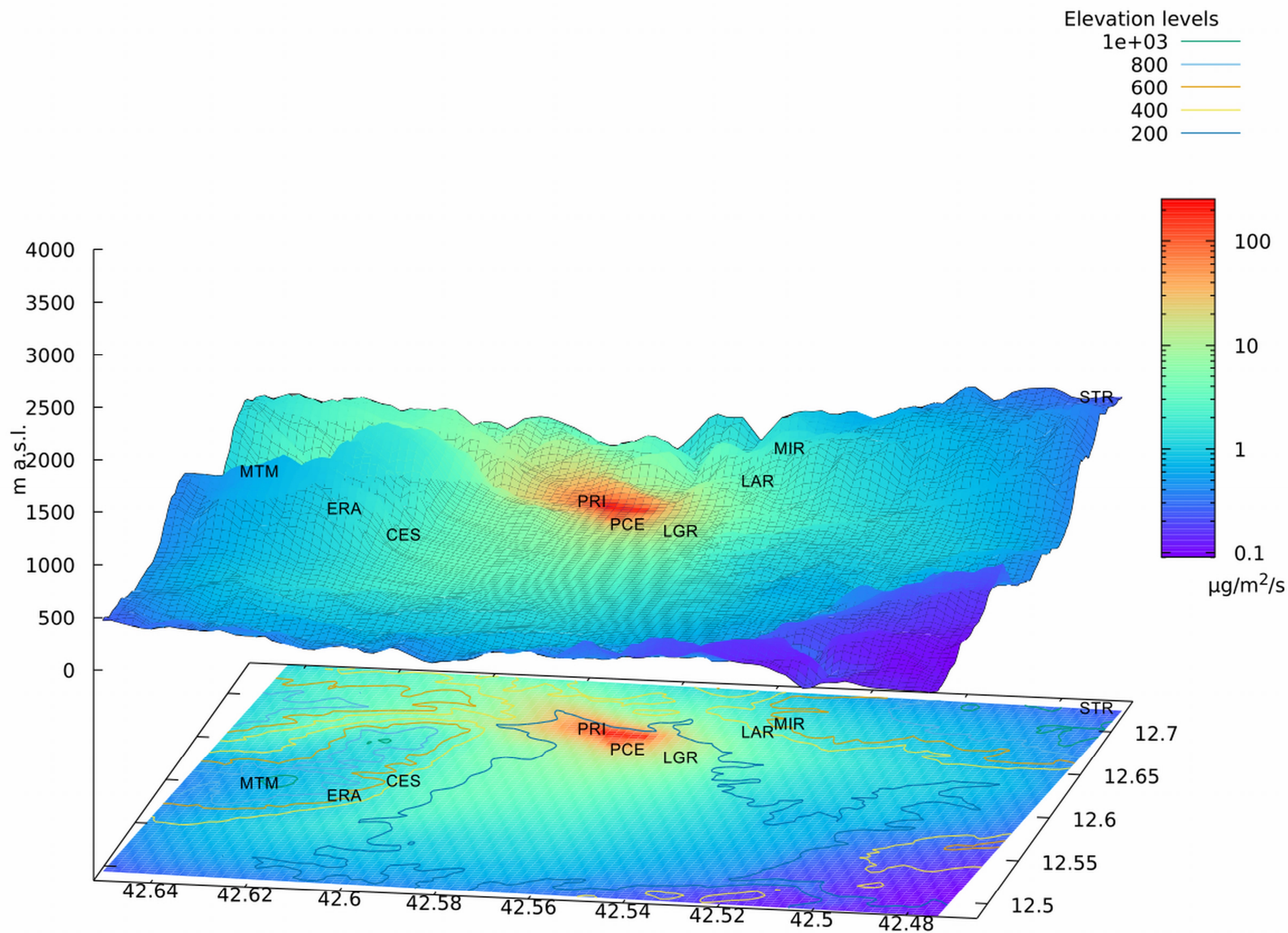


Table S1. Minimum-Maximum concentration of major element oxides (SiO₂, TiO₂, Al₂O₃, Fe₂O₃, MnO, MgO, CaO, Na₂O, K₂O, and P₂O₅; weight percent, wt %), LOI, T.O.C, N tot (weight percent, wt %), and elements (As, Ba, Br, Ce, Cl, Co, Cr, Cs, Cu, Ga, Hf, La, Mo, Nb, Nd, Ni, Pb, Rb, S, Sc, Sn, Sr, Th, U, V, W, Y, Zn, and Zr; milligrams per kilogram, mg/Kg) for each sampling station

	MM	MTM	ERA	CES	PRI	PCE	LGR	LAR	MIR	STR
SiO₂ (wt%)	28.3 - 34.5	41.3 - 42.2	32.1 - 40.5	32.4 - 36.5	33.5 - 36.1	5.8 - 11.2	53.5 - 54.6	37.6 - 40.8	50.7 - 60.7	65.7 - 70.6
TiO₂	0.73 - 0.85	0.74 - 0.76	0.39 - 0.48	0.55 - 0.63	0.39 - 0.42	0.17 - 0.21	0.64 - 0.66	0.47 - 0.51	0.54 - 0.58	0.5 - 0.56
Al₂O₃	12.7 - 15.5	14.9 - 15.8	6.9 - 8.7	9.5 - 11.3	7.1 - 7.5	1.9 - 2.7	13.3 - 13.7	8.7 - 9.7	11.6 - 13.7	11.1 - 12.4
Fe₂O₃	8.7 - 10.3	9.2 - 9.5	4.1 - 5.3	4.8 - 5.5	5.3 - 5.9	2.1 - 2.4	4.9 - 5.1	4.8 - 5.4	5.3 - 5.7	4.7 - 5.0
MnO	0.5 - 0.5	0.46 - 0.47	0.3 - 0.33	0.13 - 0.15	0.16 - 0.17	0.07 - 0.08	0.13 - 0.13	0.13 - 0.13	0.15 - 0.22	0.12 - 0.13
MgO	3.1 - 3.4	2.34 - 3.37	3.55 - 4.21	2.31 - 2.38	1.87 - 1.98	1.29 - 1.54	2.37 - 2.52	1.23 - 2.34	1.24 - 1.32	0.78 - 1.45
CaO	1.6 - 7.1	0.8 - 1.8	6.6 - 19.1	13.6 - 16.9	21.7 - 23.2	42.3 - 49.2	6.2 - 6.8	14.8 - 20.0	1.2 - 1.6	0.6 - 0.7
Na₂O	0.1 - 0.11	0.09 - 0.14	0.14 - 0.16	0.2 - 0.23	0.2 - 0.24	0.17 - 0.24	0.52 - 0.55	0.06 - 0.15	0.1 - 0.11	0.13 - 0.19
K₂O	1.83 - 1.94	1.76 - 1.86	0.93 - 1.23	1.72 - 1.89	1.24 - 1.33	0.36 - 0.56	1.83 - 1.93	1.89 - 1.98	1.14 - 1.21	1.43 - 1.54
P₂O₅	0.22 - 0.23	0.23 - 0.27	0.85 - 0.9	0.26 - 0.36	0.17 - 0.17	0.19 - 0.24	0.2 - 0.25	0.15 - 0.17	0.12 - 0.15	0.09 - 0.13
LOI	32.9 - 36.1	24.5 - 28.0	31.0 - 31.6	24.3 - 34.4	25.7 - 26.3	37.1 - 40.0	14.5 - 16.1	23.6 - 25.8	16.1 - 27.2	9.5 - 14.0
T.O.C.	7.6 - 12.0	6.3 - 9.0	6.8 - 11.5	3.2 - 10.1	1.6 - 1.9	0.9 - 2.4	1.4 - 2.4	1.7 - 5.5	4.0 - 9.7	2.1 - 4.5
N tot	0.91 - 1.14	0.75 - 0.96	0.99 - 1.37	0.38 - 1.06	0.17 - 0.24	0.11 - 0.29	0.15 - 0.23	0.2 - 0.49	0.32 - 0.68	0.22 - 0.41
As (mg/kg)	12 - 13	15 - 16	22 - 27	14 - 15	14 - 16	8 - 10	13 - 16	12 - 15	34 - 38	15 - 17
Ba	471 - 570	418 - 447	298 - 443	368 - 396	340 - 369	250 - 261	447 - 486	215 - 263	299 - 346	304 - 343
Br	14 - 24	10 - 17	6 - 7	7 - 8	3 - 4	4 - 4	3 - 4	3 - 4	5 - 6	5 - 6
Ce	156 - 193	177 - 193	58 - 83	78 - 89	50 - 66	19 - 28	84 - 98	57 - 78	157 - 175	109 - 124
Cl	5 - 5	5 - 5	5 - 5	5 - 5	25 - 55	5 - 5	18 - 19	17 - 49	11 - 25	10 - 18
Co	58 - 72	49 - 51	10 - 18	15 - 17	12 - 12	1 - 1	16 - 17	10 - 15	30 - 31	19 - 20
Cr	85 - 90	61 - 62	42 - 48	64 - 68	415 - 444	57 - 203	69 - 73	43 - 58	33 - 44	27 - 32
Cs	6 - 14	10 - 14	4 - 6	8 - 10	2 - 10	2 - 3	8 - 9	2 - 7	9 - 12	8 - 9
Cu	107 - 112	83 - 99	114 - 121	140 - 181	81 - 87	48 - 60	87 - 90	105 - 112	70 - 76	28 - 31
Ga	18 - 20	16 - 17	10 - 11	12 - 14	10 - 10	4 - 6	14 - 15	10 - 12	13 - 14	11 - 13
Hf	3 - 5	2 - 5	2 - 2	2 - 5	2 - 4	2 - 5	3 - 5	2 - 2	2 - 4	3 - 4
La	129 - 147	153 - 175	48 - 68	60 - 63	40 - 44	8 - 16	53 - 57	36 - 50	115 - 140	70 - 84
Mo	0 - 2	1 - 2	1 - 2	1 - 2	8 - 9	1 - 3	1 - 2	0 - 0	2 - 2	2 - 2
Nb	15 - 17	15 - 16	8 - 9	13 - 14	11 - 13	7 - 8	14 - 15	11 - 12	14 - 15	13 - 15
Nd	88 - 110	98 - 108	29 - 41	33 - 43	25 - 39	7 - 12	37 - 46	29 - 42	74 - 85	47 - 54
Ni	139 - 167	133 - 147	38 - 61	48 - 52	88 - 93	12 - 29	58 - 59	35 - 48	69 - 74	47 - 51
Pb	36 - 56	50 - 86	296 - 449	44 - 60	64 - 74	41 - 53	60 - 342	31 - 37	71 - 100	42 - 65
Rb	120 - 158	132 - 142	73 - 116	91 - 96	51 - 52	17 - 28	107 - 111	61 - 76	127 - 172	92 - 98
S	630 - 720	540 - 620	850 - 1040	500 - 1030	400 - 470	1070 - 1330	230 - 280	310 - 390	190 - 360	151 - 290
Sc	9 - 10	6 - 24	7 - 9	7 - 9	6 - 7	2 - 2	4 - 11	6 - 10	2 - 14	2 - 16
Sn	2 - 6	4 - 5	6 - 12	4 - 8	4 - 9	6 - 14	7 - 11	2 - 5	3 - 6	1 - 4
Sr	62 - 84	57 - 62	66 - 83	93 - 95	238 - 255	373 - 422	142 - 153	109 - 127	51 - 53	91 - 108
Th	8 - 13	10 - 14	4 - 9	13 - 23	14 - 16	2 - 14	12 - 26	4 - 10	28 - 36	20 - 26
U	3 - 4	2 - 3	1 - 2	2 - 3	3 - 3	2 - 3	2 - 2	2 - 3	2 - 3	2 - 4
V	111 - 122	93 - 101	40 - 51	69 - 79	64 - 72	29 - 32	74 - 83	62 - 71	74 - 83	70 - 80
W	5 - 6	5 - 6	2 - 3	1 - 4	1 - 2	1 - 1	2 - 3	1 - 2	4 - 6	1 - 3
Y	85 - 99	99 - 124	33 - 42	34 - 39	27 - 28	9 - 12	34 - 38	31 - 34	78 - 87	48 - 56
Zn	128 - 225	142 - 151	180 - 245	83 - 102	158 - 219	59 - 93	103 - 115	65 - 80	82 - 95	84 - 94
Zr	116 - 131	127 - 137	68 - 86	130 - 147	121 - 128	70 - 83	171 - 185	95 - 109	136 - 150	155 - 178

Table S2. Minimum-Maximum radionuclides concentration data analysed in Terni soils (becquerel per kilogram, Bq/Kg)

	MM	MTM	ERA	CES	PRI	PCE	LGR	LAR	MIR	STR
234Th (Bq/kg)	20 - 1112	0 - 451	9 - 455	0 - 30	16 - 3015	0 - 1799	24 - 3169	15 - 1486	26 - 4043	39 - 5266
226Ra	46 - 67	34 - 49	22 - 56	36 - 68	28 - 60	16 - 51	36 - 66	26 - 40	50 - 88	59 - 90
214Pb	0 - 15	7 - 33	11 - 16	1 - 26	9 - 25	0 - 22	11 - 39	3 - 12	1 - 23	26 - 49
214Bi	1 - 15	0 - 27	11 - 25	1 - 27	1 - 22	0 - 26	9 - 35	0 - 12	1 - 20	17 - 44
210Pb	24 - 111	31 - 132	46 - 92	34 - 139	39 - 53	15 - 60	35 - 51	25 - 87	47 - 177	50 - 130
228Ac	52 - 61	51 - 63	27 - 35	51 - 85	33 - 45	16 - 27	44 - 68	34 - 41	90 - 95	80 - 100
212Pb	48 - 59	31 - 56	23 - 35	34 - 54	35 - 41	17 - 24	44 - 59	27 - 36	81 - 91	71 - 83
212Bi	61 - 94	38 - 73	33 - 65	4 - 74	38 - 77	2 - 41	42 - 80	35 - 54	86 - 147	93 - 111
208Tl	15 - 18	14 - 48	7 - 10	13 - 20	11 - 13	5 - 29	13 - 21	8 - 11	24 - 29	22 - 26
40K	445 - 481	389 - 451	295 - 333	409 - 531	304 - 335	151 - 199	427 - 635	399 - 461	273 - 338	381 - 509
137Cs	11 - 83	17 - 186	40 - 107	16 - 100	10 - 13	8 - 35	15 - 27	12 - 29	28 - 157	27 - 104
210Pb_{ex}	18 - 65	32 - 95	4 - 81	57 - 92	2 - 15	2 - 41	5 - 13	23 - 54	5 - 128	12 - 103

Table S3. PAHs (Naphthalene, Acenaphthene, Acenaphthene, Fluorene, Phenanthrene, Anthracene, Fluoranthene, Pyrene, Benzo(g,h,i)fluoranthene, Benzo(a)anthracene, Chrysene+Triphenylene, Benzo(b+j)fluoranthene, Benzo(k)fluoranthene, Benzo(a)fluoranthene, Benzo(e)Pyrene, Benzo(a)Pyrene, Perylene, indenofluoranthene, Indeno(1,2,3-cd)pyrene, Dibenzo(a, h)anthracene, Benzo(b)chrysene, Benzo(g,h,i)perylene, dibenzo(x,y)pyrene, and Coronene; nanograms per gram, ng/g) and n-alkanes (from C12 to C39; nanograms per gram, ng/g) concentration data analysed in Terni soils

	MM	MTM	ERA	CES	PRI	PCE	LGR	LAR	MIR	STR
Naphthalene (ng/g)	0.1	5.4	0.2	0.1	0.4	0.3	4.3	0.0	0.3	0.1
Acenaphthene	0.3	4.3	0.6	0.3	0.9	0.7	2.7	0.2	0.2	0.1
Acenaphthene	3.4	4.5	5.2	4.2	0.9	2.0	50.1	0.7	1.5	1.9
Fluorene	3.7	2.1	2.7	2.6	25.4	43.9	9.4	1.3	3.2	2.3
Phenanthrene	0.5	0.1	0.3	0.2	3.3	6.8	1.4	0.1	0.3	0.1
Anthracene	3.3	4.4	3.1	4.3	53.5	262.2	43.4	3.1	6.6	2.2
Fluoranthene	2.9	2.5	2.5	3.8	32.0	152.4	26.7	1.8	3.7	1.7
Pyrene	1.5	0.3	0.5	0.5	2.3	9.3	1.7	0.1	0.3	0.4
Benzo(g,h,i)fluoranthene	3.0	1.0	1.9	2.8	27.2	122.8	14.4	1.1	2.0	1.2
Benzo(a)anthracene	4.4	2.2	2.1	2.5	21.7	100.5	13.6	1.2	3.2	1.4
Chrysene+Triphenylene	3.4	1.2	3.9	6.1	17.2	92.4	13.8	1.5	2.7	1.8
Benzo(b+j)fluoranthene	3.0	0.6	1.8	3.8	8.7	47.6	10.5	0.9	1.9	1.4
Benzo(k)fluoranthene	0.1	0.5	0.4	0.5	3.0	24.7	3.2	0.2	0.4	0.3
Benzo(a)fluoranthene	2.8	2.5	3.9	4.3	17.7	83.8	17.0	1.8	3.5	2.2
Benzo(e)Pyrene	2.9	1.4	2.4	3.6	27.5	135.1	21.9	1.8	2.8	1.4
Benzo(a)Pyrene	3.5	0.1	1.0	0.9	5.1	27.6	4.8	0.5	0.6	0.6
Perylene	1.4	0.5	0.8	0.5	1.3	4.9	1.3	0.3	1.9	0.5
indenofluoranthene	3.7	2.7	4.0	5.5	12.7	90.0	14.4	1.6	2.7	2.2
Indeno(1,2,3-cd)pyrene	2.1	0.7	0.7	0.9	4.3	25.7	3.7	0.6	0.5	0.4
Dibenzo(a,h)anthracene	3.0	0.7	0.5	0.3	4.1	22.3	3.5	0.4	0.2	0.3
Benzo(b)chrysene	3.8	3.9	4.7	5.1	11.6	85.3	20.5	2.7	4.1	2.4
Benzo(g,h,i)perylene	0.8	4.6	1.4	1.6	15.2	29.9	12.8	1.2	2.6	0.9
dibenzo(x,y)pyrene	3.9	5.1	5.6	5.4	3.2	54.4	20.6	2.6	4.4	2.2
TOT	58.1	53.0	53.3	60.3	300.0	1426.5	321.0	26.4	50.2	32.4
C12 (ng/g)	0.43	<LoD	0.45	0.64	0.05	<LoD	<LoD	<LoD	<LoD	0.25
C13	1.32	<LoD	0.74	0.66	0.17	<LoD	<LoD	<LoD	<LoD	0.28
C14	0.31	<LoD	0.42	0.56	0.48	<LoD	<LoD	<LoD	0.20	0.51
C15	0.53	0.12	0.26	0.41	0.29	<LoD	<LoD	<LoD	0.22	0.37
C16	0.46	0.20	0.42	0.42	0.39	<LoD	0.66	<LoD	0.69	0.40
C17	1.20	0.58	0.59	1.14	1.10	0.76	1.42	0.58	1.92	0.82
C18	1.22	1.02	0.81	1.22	0.86	0.48	1.28	0.78	2.24	0.65
C19	3.06	1.45	0.86	2.60	0.79	0.45	1.59	1.63	3.86	1.09
C20	4.87	2.45	1.91	4.33	1.02	0.89	1.93	2.13	5.21	2.44
C21	12.74	5.89	3.34	14.49	4.71	2.53	2.71	5.86	6.96	4.19
C22	10.05	5.36	1.68	4.16	4.55	3.40	3.67	4.39	7.35	2.49
C23	22.31	13.21	4.73	25.07	13.57	4.86	10.14	10.13	16.35	5.01
C24	7.40	8.82	2.61	7.46	8.33	5.93	5.24	9.18	9.38	2.54
C25	46.87	30.83	14.58	47.57	30.37	9.89	19.15	33.09	31.17	12.64
C26	23.35	15.87	6.10	12.66	14.10	5.57	9.18	14.39	14.47	4.60
C27	143.80	132.53	55.71	100.30	83.91	25.23	96.32	114.79	225.49	45.97
C28	49.01	60.21	16.91	26.10	25.07	8.70	24.16	32.30	54.78	12.24

C29	344.58	290.20	232.48	322.16	225.60	75.66	123.87	396.71	947.64	78.70
C30	27.01	21.47	15.21	38.85	22.28	8.25	9.86	24.18	34.16	5.99
C31	353.88	302.09	281.35	619.09	314.12	82.45	103.39	300.93	490.49	68.38
C32	18.64	17.83	9.69	74.35	19.51	8.79	7.95	19.11	11.31	3.34
C33	153.41	142.65	106.42	571.25	95.44	36.39	31.61	110.87	51.97	27.79
C34	12.84	4.92	4.10	116.79	11.50	4.71	2.98	13.94	3.86	2.72
C35	31.94	13.32	25.09	342.83	17.24	8.33	5.78	35.15	13.58	7.73
C36	2.47	0.88	1.25	10.87	7.05	2.67	1.71	6.41	5.63	1.47
C37	1.22	2.87	2.75	7.82	6.80	3.02	2.15	5.07	1.10	1.82
C38	<LoD	<LoD	1.67	<LoD	4.17	<LoD	1.40	<LoD	<LoD	<LoD
C39	<LoD	<LoD	3.20	<LoD	2.17	<LoD	<LoD	<LoD	<LoD	<LoD
TOT	1274.93	1074.76	795.35	2353.81	915.00	298.90	468.15	1141.60	1940.04	1746.15